CLEAR ANTI-SMUDGE COATINGS OF DIBLOCK COPOLYMERS

by

Danielle Macoretta

A thesis submitted to the Department of Chemistry

In conformity with the requirements for

the degree of Master of Science

Queen's University

Kingston, Ontario, Canada

(September, 2014)

Abstract

Two poly[3-(triisopropyloxysilyl)propyl methacrylate]-*block*-poly[2-(perfluorooctyl)ethyl methacrylate] (PIPSMA-*b*-PFOEMA or P1-1/P1-2) samples and one poly(perfluoropropylene oxide)-*block*-poly-[3-triisopropyloxysilyl)propyl methacrylate] (PFPO-*b*-PIPSMA, or P2) sample were synthesized, characterized, and used to coat glass plates. The coatings were formed by evaporating a dilute copolymer solution containing an HCl catalyst to facilitate the sol-gel chemistry of the PIPSMA blocks. To minimize polymer consumption, we targeted diblock copolymer unimolecular (brush) layers that consisted of a sol-gelled PIPSMA sub-layer that was anchored onto the glass plates, and a fluorinated surface layer that provided the desired water and oil repellency. A systematic study was performed examining the effect of varying the catalyst amount, the polymer amount, and the block copolymer composition on the structure, morphology, and water- and oil- repellency of the coatings. The amphiphobicity of the coatings improved initially with the amount of grafted polymer, but plateaued once a saturated brush layer was formed. Furthermore, the static contact angles (SCAs) increased as the relative length between the PFOEMA and PIPSMA blocks increased. All of the coatings were optically clear and repelled ink from a permanent Sharpie® marker. The markings that were left behind were the faintest on the P2 coatings as the ink would instantaneously shrink into patches. In addition, the P2 coatings exhibited far better wear-resistance than the P1-1/P1-2 coatings. The anti-smudge properties of the coatings should facilitate their use on touch screens of hand-held electronic devices such as iPads® and iPhones®.

Acknowledgements

I would firstly sincerely wish to thank Dr. Guojun Liu for all of his undying support, patience and guidance through this challenging yet rewarding process. I thoroughly enjoyed working under his supervision, and cannot express how thankful to him I am for graciously welcoming me into his group, and providing me with this amazing opportunity.

I would also like to express my gratitude to all of the past and present members of the Liu Group during my time in the lab: Yu Wang, Weijie Jiang, Heng Hu, Bolu Peng, Prashant Agrawal, Dr. Xiaoyu Li, Dr. Zengqian Shi, Dr. Ian Wyman, Dr. Claudia Grozea, Dr. Muhammad Rabnawaz, Dr. John Dupont, Dr. Ganwei Zhang and Jian Wang. Your support and kindness has made this experience unforgettable. I wish to extend special thanks to Yu Wang for all of his hard work in training me, and for smiling every day; Jian Wang for teaching me how to operate and run the AFM correctly and efficiently; Muhammad Rabnawaz for synthesizing and characterizing all of the diblock copolymers discussed in this thesis; Claudia Grozea for doing a fabulous job assisting me with my paper and being a great female support; and Ian Wyman for proofreading this thesis.

I would like to show my appreciation for the Department of Chemistry, and Queen's University for providing me with an amazing opportunity to participate in cutting-edge scientific research. I have met so many amazing people, and will keep them close to my heart.

I would like to recognize the natural sciences and engineering research council (NSERC) as well as the other funding agencies that have enabled me to conduct this great research. Without them, I would not have had access to the materials and instruments necessary for this research.

I would also like to thank my wonderful boyfriend William, for giving me endless long-distance support through this process. He has been amazing through these two years of my life.

Last, but certainly not least, I would like to thank my family for their continued love and support in everything I do. I would not be here without them.

Table of Contents

List of Figures

List of Tables

List of Abbreviations

γ	interfacial tension
γ_{LG}	interfacial energy of a liquid/gas interface
γ_{SG}	interfacial energy of a solid/gas interface
γ_{SL}	interfacial energy of a solid/liquid interface
γ-APS	3-aminopropyltriethoxysilane
θ	static contact angle
θ*	apparent contact angle
θ_o	intrinsic contact angle
θ_{adv}	advancing contact angle
θ_{rec}	receding contact angle
θ_s	sliding angle
ρ	density
AFM	atomic force microscopy
ATRP	atom transfer radical polymerization
ARCA	advancing receding contact angle method
C_6F_6	hexafluorobenzene
CA	contact angle
CAH	contact angle hysteresis
$CDCl_3$	deuterated chloroform
DRIFT-IR	diffuse reflectance infrared Fourier-transform spectroscopy
FL_m	fluorinated block with *m* units as part of the diblock copolymer structure GX_n-*b*-FL_m

f_{SL}	area fraction of a liquid droplet in contact with a surface
GX_n	grafting/crosslinking block with *n* units as part of the diblock copolymer structure GX_n-*b*-FL_m
H_2O_2	hydrogen peroxide
H_2SO_4	sulfuric acid
HCl	hydrochloric acid
KBr	potassium bromide
M-O-M	metal-oxygen-metal bond
M_n	number average molecular weight
M_w	weight average molecular weight
NMR	nuclear magnetic resonance
P1-1	$PIPSMA_{18}$-*b*-$PFOEMA_{22}$
P1-2	$PIPSMA_{13}$-*b*-$PFOEMA_{30}$
P2	$PFPO_{14}$-*b*-$PIPSMA_7$
PEO	poly(ethylene oxide)
PFOEMA	poly[2-(perfluorooctyl)ethyl methacrylate]
PFPE	perfluoropolyether
PFPO	poly(perfluoropropylene oxide)
PIPSMA	poly-[3-(triisopropyloxysilyl)propyl methacrylate]
PS	polystyrene
r	roughness factor
R_{rms}	root mean square roughness
SA	sliding angle
SCA	static contact angle

SEC	size exclusion chromatography
-Si(OR)$_3$	trialkoxysilane group
Si-OH	silanol group
Si-O-Si	siloxane bond
SLIPS	slippery liquid infused porous surfaces
TD	tilting drop method
TEOS	tetraethyl orthosilicate
TFT	α,α,α-trifluorotoluene
T_g	glass transition temperature
THF	tetrahydrofuran
UV-Vis	ultraviolet- visible spectroscopy
XPS	X-ray photoelectron spectroscopy

Chapter 1

Introduction

1.1 Research Objectives and Organization of the Thesis

Diblock copolymers GX_n-*b*-FL_m that consist of a grafting/crosslinking block of *n* GX units covalently attached to a fluorinated block of *m* FL units can form a brush (or unimolecular) layer covering a solid substrate. In this layer, the GX block becomes grafted and crosslinked onto the substrate, while the overlaying low-surface-tension FL block provides the desired repellency against water- and oil- borne contaminants. The specific GX_n-*b*-FL_m samples that were used in this study were poly-[3-(triisopropyloxysilyl)propyl methacrylate]-*block*-poly[2-(perfluorooctyl)ethyl methacrylate] ($PIPSMA_{18}$-*b*-$PFOEMA_{22}$, also denoted as P1-1), $PIPSMA_{13}$-*b*-$PFOEMA_{30}$ (P1-2), and poly(perfluoropropylene oxide)-*block*-poly-[3-(triisopropyloxysilyl)propyl methacrylate] ($PFPO_{14}$-*b*-$PIPSMA_7$, or P2), where the subscripts denote the numbers of repeat units for the different blocks (Figure 1-1). Specifically, these diblock copolymers were grafted onto glass surfaces via the sol-gel chemistry of the PIPSMA block. The sol-gel process involved both a hydrolysis and a condensation reaction, which occurred simultaneously.[1] This process is illustrated in Figure 1-2. In the presence of an acid catalyst, hydrolysis caused the triisopropyl groups to become cleaved from the PIPSMA block, thus producing silanol groups (Si-OH). During the condensation reaction, the Si-OH groups reacted with other Si-OH groups present on the surface of the glass, or with other Si-OH groups of the hydrolyzed polymer to form a network of siloxane bonds (Si-O-Si).

The P1-1 and P1-2 copolymers of the PIPSMA-*b*-PFOEMA family were compared to examine the effect of varying the block length ratio on the surface properties of the resultant coatings. In addition, the PIPSMA-*b*-PFOEMA and PFPO-*b*-PIPSMA families were compared to investigate how the flexibility of the fluorinated block affected the properties of the coatings. For example, while PFOEMA forms a

smectic-A liquid crystalline phase at room temperature[2] and has a smectic-A-to-disorder transition temperature of 76 ˚C,[3-4] PFPO is a liquid at room temperature and has a glass transition temperature (T_g) of -71 ˚C.[5]

The water- and oil- repellent coatings described in this work can be applied onto glass substrates to produce films that are smooth, ultrathin, optically clear, and that demonstrate anti-smudge properties. These are coatings that repel water and oil borne contaminants alike. They can thus be applied onto various glass-based substrates. For example, these coatings are promising candidates for applications on the touchscreens of electronic devices such as iPads® and iPhones®.

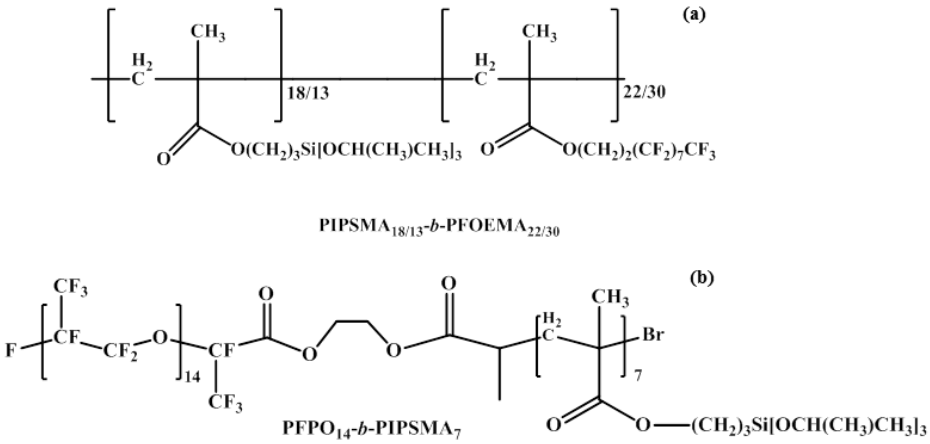

Figure 1-1 Chemical structures of P1-1/P1-2 (a) and P2 (b).

This chapter provides general background information describing water- and oil- repellent surfaces, and the key factors that influence their performance. Furthermore, important information regarding dynamic non-wetting surfaces and the various ways to prepare these materials will be described. The preparation of polymer brushes and the sol-gel reaction process will also be described in this chapter. Chapter 2 will briefly outline the characterization details regarding the diblock copolymers P1-1/P1-2 and P2, and subsequently their use in the preparation of amphiphobic brush coatings covering glass surfaces. Various characterization techniques used during this project included diffuse reflectance infrared Fourier-transform spectroscopy (DRIFT-IR), atomic force microscopy (AFM), X-ray

photoelectron spectroscopy (XPS), ultraviolet- visible spectroscopy (UV-Vis) and will also be included in Chapter 2 together with the protocols for various contact angle measurements. Chapter 3 will focus on the results and discussion, including details on the effect of varying the catalyst amount, polymer amount, and block copolymer composition on the structure, morphology, and repellency of the resultant coatings. The summary and conclusions, as well as the proposed future work will be presented in Chapter 4.

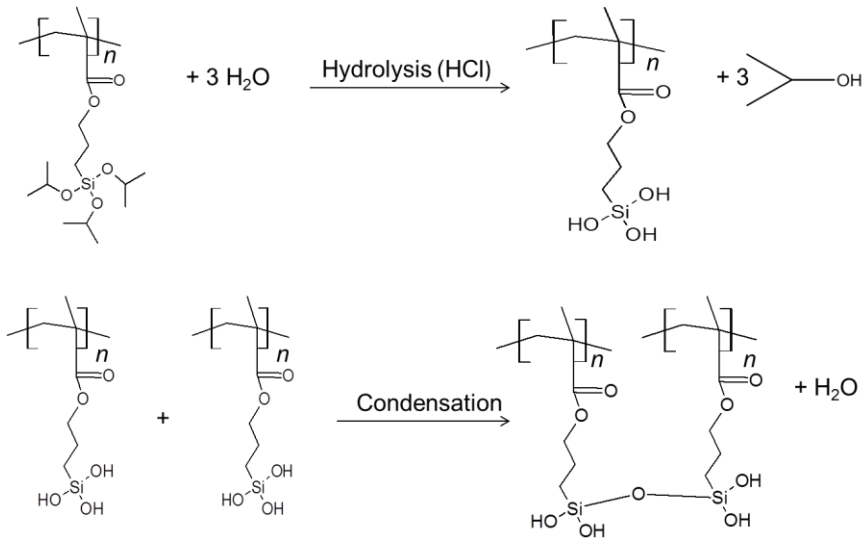

Figure 1-2 Schematic diagram of the sol-gel process occurring in this system.

1.2 Introduction to Water- and Oil- Repellent Surfaces and Their Applications

1.2.1 General Definition of Hydrophobic Surfaces and Their Applications

When a water droplet displays a static contact angle (SCA) > 90˚ on a surface, that substrate is typically defined as a hydrophobic surface. On the other hand, when a water droplet displays a SCA < 90˚ on a surface, the substrate is typically defined as a hydrophilic surface.[6] The SCA is defined as the angle formed by a liquid at the three phase boundary where the solid (S), liquid (L), and gas (G) phases all intersect. The interfacial energies of the solid/liquid, liquid/gas, and solid/gas interfaces are denoted as

γSL, γLG, and γSG, respectively.[7-8] Figure 1-3 illustrates the SCA of a water droplet sitting on a flat surface.

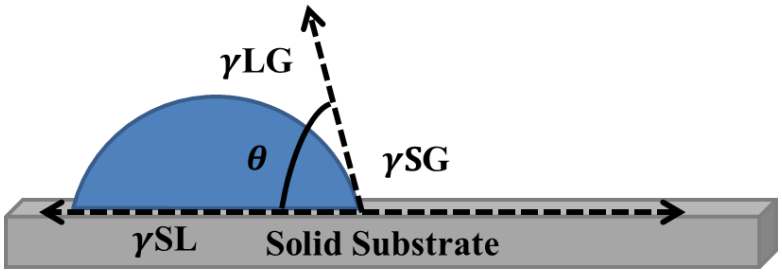

Figure 1-3 SCA of a water droplet on a flat surface.

Although a self-cleaning surface should ideally exhibit a high SCA, this property alone does not completely determine the self-cleaning capabilities of a surface.[9] In many circumstances, the surface wettability and self-cleaning capabilities are tested by measuring the SCA in combination with other dynamic CA measurements (modification of the droplet).[10] These measurements include the contact angle hysteresis (CAH) and the sliding angle (SA). The CAH is generally defined as the difference between the advancing CA (θ_{adv}) and the receding CA (θ_{rec}), or it can also be defined as ($\cos\theta_{rec}$ - $\cos\theta_{adv}$).[11] When a small amount of liquid is added to an existing droplet on a surface, the SCA will increase, but the interfacial area at the liquid/solid interface may remain constant. The maximum SCA achieved without changing the interfacial area corresponds to θ_{adv}. On the other hand, when a small amount of liquid is removed from an existing droplet, the SCA will decrease, but the interfacial area at the liquid/solid interface may remain constant. The minimum SCA achieved without changing the interfacial area corresponds to θ_{rec} (Figure 1-4a).[10,12] Another way of measuring θ_{adv} and θ_{rec} is demonstrated in Figure 1-4b. On a tilted substrate, the maximum and minimum SCAs achieved just before the droplet slides, are θ_{adv} and θ_{rec}, respectively.[11-12] If the CAH is sufficiently low, a liquid droplet may slide, even on a flat substrate. However, in most cases, the liquid will not slide on a flat surface unless it is tilted at a certain angle relative to the horizontal plane. The SA (θ_s) is generally recorded as the angle at which the sliding

occurs[13] (Figure 1-4c). Self-cleaning and dynamic non-wetting surfaces typically have high SCA values and low CAH and SA values.[10]

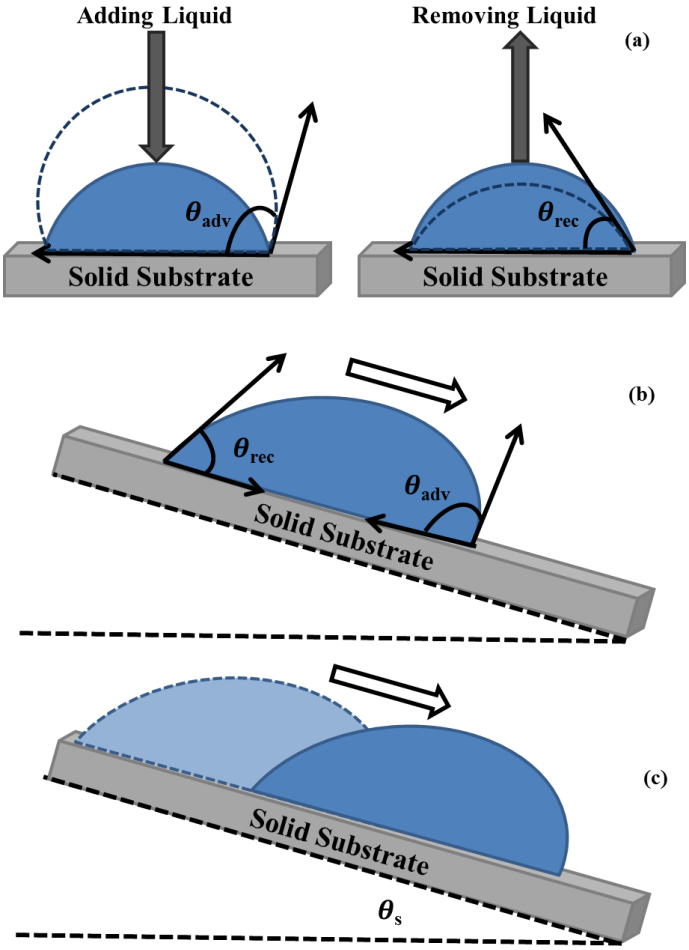

Figure 1-4 A schematic representation of the dynamic CA measurements to determine the wettability and self-cleaning properties of a surface. The θ_{adv} and θ_{rec} values can be measured by adding and removing liquid to and from an existing droplet (a), or by placing a droplet on a flat substrate that can be tilted (b). The θ_s (c) is the angle at which the droplet slides down the substrate.

Hydrophobic materials are promising candidates for non-wetting surfaces with various applications in our everyday life. For example, they have been used for drag reduction, anti-fogging, anti-bacterial, anti-fouling, anti-icing, and corrosion resistance applications.[10,14-15] Although high water repellency is highly desirable, the hydrophobic and self-cleaning properties of these surfaces can be

compromised when alcohol or other oil-based liquids are introduced to them.[16] A prime example of this phenomenon was encountered in 2010 when the Gulf of Mexico experienced the worst oil spill disaster in US history.[17] This tragic event killed many birds despite the fact that their feathers were hydrophobic. If any of these organisms and habitats could have repelled oil, this event would potentially not have had such dire consequences, as the oil would not have had a chance to wet their wings in the first place. To this day, the Gulf of Mexico is still not clean. Thus, it is important to gain insight about surfaces that have repellency against liquids other than water alone.

1.2.2 General Definition of Oleophobic Surfaces and Their Applications

A surface that repels an oil droplet with a SCA > 90˚ is considered to be oleophobic, whereas a surface that repels an oil droplet with a SCA < 90˚ is considered to be oleophilic.[6] There have been many reviews describing hydrophobic surfaces in the past,[18-21] but very few have focused on oleophobic surfaces.[10,22-23] However, their range of applications are more diverse than those of hydrophobic materials.[10] Some of the more important examples include water/oil separations, anti-crawling materials, marine anti-fouling materials, fluid power systems, protection of oil pipelines against clogging, resistance against wax deposition in fuel oil tanks, and anti-bioadhesion.[24-27]

Although hydrophobic and oleophobic surfaces are highly desirable, the concept of a dual repellent surface that could repel both water and oily liquids simultaneously would be even better. Such a coating could be applied onto the screens of a small electronic device such as an iPad® or an iPhone®, for example. It would be ideal for protecting a device against oily fingerprints and spills. The work presented in this thesis has the potential for applications such as this.

1.2.3 General Definition of Amphiphobic Surfaces and Their Applications

Surfaces that simultaneously exhibit water and oil with SCAs > 90˚ are known to be amphiphobic.[6,28] The preparation and use of these surfaces are highly desirable as they combine efficiency and convenience for consumers everywhere. Self-cleaning, anti-fouling, corrosion resistant, and anti-bacterial properties are just a few examples of their capabilities.[29-33,34-35] Although it can be difficult to prepare such coatings due to the low surface tension of some oils,[36] there is a great demand for these materials. Consequently, the preparation of these surfaces has been the focus of cutting-edge research throughout the world.

1.3 Key Parameters for Preparing Water- and Oil- Repellent Surfaces

Much research in this field has been devoted toward the imitation of structures observed in nature. Scientists are highly interested in reproducing surfaces similar to that of the distinguished lotus flower (*Nelumbo nucifera*) due to its spectacular self-cleaning capabilities.[37] The leaves of this plant are able to bead up rain droplets and the beaded droplets can roll away with dirt and bacteria. Thus, these leaves are self-cleaning. Other natural examples of this kind include the legs of a water strider, the leaves of a rice plant, rose petals, fish scales, shark skin, and butterfly wings.[37-41] In order to mimic the surfaces seen in nature, a number of key factors must be investigated. The surface free energy, and the surface geometrical structure are the two most important parameters that affect the wettability of a surface.[10] A material with a low surface free energy is primarily needed to render surfaces water- and oil- repellent. Meanwhile, a surface should possess a combination of a low surface free energy, enhanced surface roughness, and re-entrant surface structures in order for that material to exhibit higher liquid repellency as well as good dynamic properties. These latter surfaces can exhibit CAs > 150˚ with a CAH typically < 10˚ and are commonly referred to as superamphiphobic surfaces.[10] While superamphiphobic materials may exhibit better self-cleaning properties than amphiphobic surfaces, superamphiphobic materials can be

costly to prepare. Consequently, superamphiphobic materials may be more suitable for specialized applications, while amphiphobic materials may have greater potential for routine or cost-sensitive applications. It is important to note that the work described in this thesis strictly refers to smooth amphiphobic surfaces with low surface energies. However, a brief introduction to surface roughness and re-entrant surface structures is also included to obtain a better understanding of the concepts of self-cleaning surfaces.

1.3.1 Surface Energy

The chemical composition of a material defines its surface energy, which strongly influences the wetting properties of that material.[42] The primary measure of a liquid droplet on a flat, smooth, and chemically homogenous surface is the SCA, θ, given by Young's relationship shown in Equation 1-1.[43] Here, γ refers to the interfacial tension, and the subscripts S, L, and G refer to the solid, liquid and gas phases, respectively.

$$\cos\theta = \frac{\gamma_{SG} - \gamma_{SL}}{\gamma_{LG}} \qquad (1\text{-}1)$$

According to the Young equation, a material that has a lower γ_{SG}value or a lower surface free energy tend to result in higher liquid repellency.[42] As mentioned earlier, it is often difficult and costly to prepare a superamphiphobic surface. This is because in order for oils with low surface tensions to be repelled, the surface energy of the material (γ_{SG}) must be lower than 7.5 mN/m.[44-46] To date, the -CF_3 groups of fluorine-containing compounds are the only functional groups that will yield such a low surface energy.[47] Zisman *et al.* reported that the surface free energy of a material decreased in the order of -CH_2 > -CH_3 > -CF_2 > -CF_2H > -CF_3.[48] The effect of fluorine lowering the surface energy originates from the fact that fluorine has a small radius, and the greatest electronegativity among all of the atoms. Consequently, it

forms with carbon a stable covalent bond that is not easily polarizable, and the London dispersion forces and Debye forces among different fluorinated hydrocarbons tend to be low.[49] The -CF_3 groups of a fluorinated alkane monolayer may pack hexagonally on a surface and have provided the lowest reported surface free energy of any solid with a value of 6.7 mN/m.[47,49-50] On a smooth surface such as this, it is possible to obtain maximum water (72.9 mN/m) and diiodomethane (50.8 mN/m) SCAs of 120˚ and 100˚, respectively.[51-52] Lowering the surface free energy of a smooth coating is sufficient to render amphiphobic properties, but in order to create surfaces with much higher liquid repellency, surface roughness and re-entrant surface structures need to be introduced.[10]

1.3.2 Surface Roughness and Re-entrant Surface Structures

In addition to a low surface free energy, the introduction of roughness can enhance the overall liquid repellency of a surface. Adding roughness to a surface increases the actual surface area of the material in relation to the flat projected area of the same material. A larger surface area as well as a lower surface free energy diminishes the likelihood of the droplet spreading, and therefore increases the apparent CA of the liquid droplet. In this case, the apparent CA (θ^*) is the angle observed on a textured or rough surface. Consequently, introducing roughness to a surface can increase the CA between a liquid and a flat surface if the intrinsic CA is > 90˚. The intrinsic contact angle (θ_o) is defined as the SCA observed when a droplet is on a flat surface of the same material.

When a liquid droplet is placed on a textured or rough surface, there are two different scenarios that could take place in an effort to reduce its overall free energy. The first scenario (Figure 1-5a) is observed when the droplet fully penetrates the grooves and cavities of the roughened surface, which ultimately forms a "fully-wetted" interface. When the droplet assumes this configuration, it is known to be in the Wenzel State.[53] In this state, the apparent CA can be calculated using Equation 1-2.

$$\cos\theta^* = r\cos\theta_o. \qquad (1\text{-}2)$$

As shown here, r is the roughness factor, which is defined as the ratio of the actual surface area of the rough surface divided by its flat projected area of the same material. Since the r factor will always be greater than 1, roughness can enhance both the wetting and non-wetting properties of a surface. Meanwhile, $\theta^* > \theta_o$ will occur when $\theta_o > 90^\circ$, and $\theta^* < \theta_o$ will be observed when $\theta_o < 90^\circ$.[32]

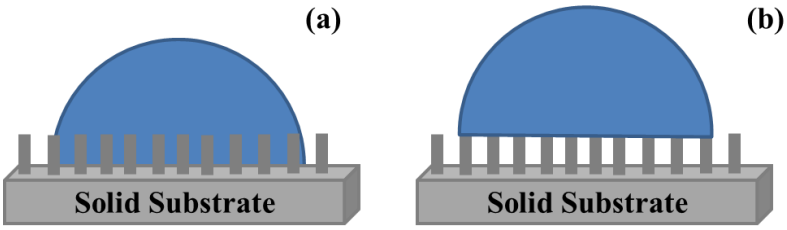

Figure 1-5 Schematic depiction of a liquid droplet in the Wenzel State (a) and Cassie State (b).

On the other hand, the second scenario (Figure 1-5b) is encountered when the liquid droplet does not fully penetrate the cavities, but instead sits on top of air that is trapped inside them. A solid/liquid/air composite interface is then formed. When the droplet assumes this configuration, it is said to be in the Cassie State. This relationship is expressed by Equation 1-3.[54]

$$cos\theta^* = r f_{SL} cos\theta_o - (1 - f_{SL}) \qquad (1\text{-}3)$$

In this case, f_{SL} and $1 - f_{SL}$ refer to the area fraction of the liquid droplet in contact with the surface, and the area fraction of the liquid droplet in contact with the trapped air, respectively. An increase in f_{SL}so that it approaches 1 indicates that there is a decrease in the amount of air trapped below the droplet. As this trend occurs, the droplet will begin to penetrate into the cavities, transitioning into the Wenzel State. As mentioned earlier in this chapter, a high SCA alone is not sufficient to determine the wettability of a surface. It is important to have a low SA and CAH. A droplet is more likely to roll off a

surface if it is in the Cassie State versus when it is in the Wenzel State. This is purely due to the fact that there is less adhesion of the droplet to the substrate in the Cassie State, and weaker van der Waals interactions.[53-54] Typically, droplets sitting on superamphiphobic surfaces are in the Cassie State, but it is still possible for a droplet to become unstable in this situation if the CA < 90˚. In recent years, re-entrant surface structures have been recognized to be important in ensuring that droplets remain in the Cassie State[23] on superamphiphobic surfaces.

The main difference between amphiphobic and superamphiphobic surfaces is that amphiphobic surfaces generally do not possess much roughness, and they typically do not possess re-entrant surface structures. These kinds of surfaces are hidden under overhangs with examples including mushroom-like posts, or inversed trapezoidal pillars as reported by Tuteja *et al.*[23,55-56] An example of such a structure is illustrated in Figure 1-6. Re-entrant surface structures encourage the liquid to remain above the composite interface because as the liquid droplet naturally presses down against the surface (Figure 1-6a), f_{SL} will decrease, and θ^* will increase. In the absence of re-entrant surface structures (Figure 1-6b), f_{SL} will increase as the liquid presses down on the surface, and hence θ^* will decrease. With the use of re-entrant structures (Figure 1-6a), it is more likely that the liquid droplet will remain in the Cassie State rather than undergo a transition to the Wenzel State because the downward movement of the liquid/solid/air interface decreases f_{SL} and increases θ^* calculated from Equation 1-3.

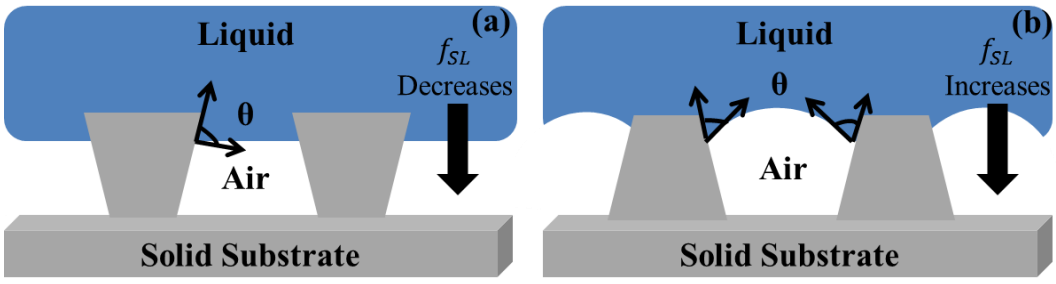

Figure 1-6 Cross sectional figure of surfaces with re-entrant surface curvature structures (a), and without re-entrant surface curvature structures (b).

In this work, smooth amphiphobic surfaces were prepared using diblock copolymers that consisted of both a GX and a FL block. These copolymers were applied onto glass plates. The GX block served as the anchoring block, while the exposed FL block provided the coating with a low surface energy. Due to this low surface energy, these coatings exhibited dynamic non-wetting properties to allow water and oils to slide off their surfaces.

1.4 Dynamic Non-Wetting Surfaces

It has been reported that the droplet mobility on a surface or coating is independent of the SCA, but highly dependent on the CAH and the dynamic properties of the surface.[9] Coatings that repel water- and oil- borne contaminants alike are referred to as anti-smudge coatings. Anti-smudge coatings are currently prepared through three approaches. As mentioned earlier, the first approach deals with the production of superamphiphobic surfaces. The coating is composed of surface-fluorinated nano- and/or micro-architectures.[57-64] While fluorination decreases the surface tension, the architectures render the high surface area (roughness) and re-entrant sites required to repel a testing liquid.[65-67] In the second approach, the coating is made of a porous matrix such as a fluorinated sponge that is filled with a low surface-tension fluorinated oil such as Krytox.[68-69] While the oil is held in position due to its affinity for the porous matrix, the incompatibility between the oil and a test liquid minimizes the penetration of the latter into the former. These systems are referred to as slippery liquid infused porous surfaces or SLIPS.[70] The third approach bears resemblance to the second approach, where it also uses a fluorinated oil. However, the fluorinated oil such as a perfluoropolyether (PFPE) is covalently grafted upon a substrate in this case instead of being infused inside.[9,71-73] In the case of a flat substrate, the coating/testing liquid interface is flat just as that found in the second approach.

Coatings prepared through the first approach can typically have SCAs that exceed 150˚ for liquids ranging from water to hexadecane with room-temperature surface tension values of 72.9 and 27.5 mN/m, respectively.[52] Liquid droplets readily roll off of these superamphiphobic coatings because the contact

area and thus the van der Waals adhesion forces between a beading test liquid drop and the coating are small. On the other hand, test liquids such as water or hexadecane placed on the flat coatings prepared through the second and third approaches display CAs that never exceed ~120˚. A test liquid slips readily off these surfaces because the coating is physically and chemically homogeneous. Because it is physically homogeneous, the surface of the coating is almost molecularly smooth with no "permanent" solid obtrusions that exist to pin down the contact lines formed between the test liquid droplets and the coating. Rather, molecules both in the coating and in the test liquid around the contact line are in constant motion, causing the interaction between the droplet and the surface to be dynamic. The motions of the oil molecules also ensure the chemical homogeneity of the coating. As long as the coating layer is sufficiently thick to fully cover the substrate or the grafting functionalities that may pin the test droplet, the test liquid at every contact point experiences the same time-average composition for the oil. It is well known that the CAH diminishes on a homogeneous surface.[74-75] Furthermore, a test liquid may slide off such a surface if it is slightly tilted. Thus, the second and third approaches offer coatings with dynamic non-wetting behaviour against water and hydrocarbon droplets and will be the focus of this work.

The third approach produces unimolecular thin coatings that should be optically clear unlike those provided by the first and second approach. A clear anti-smudge coating on a flat substrate such as glass has many potential applications. For example, such a coating on window glass of skyscrapers reduces the frequency of window washing and saves costs. Such a coating on the touch screen of an iPad® or iPhone® rejects fingerprints and maintains the aesthetic appeal of the device.

Traditionally, perfluoropolyethers (PFPEs) have been grafted onto glass plates via the sol-gel chemistry of one terminal trimethoxysilane or triethoxysilane group or a trialkoxysilane group $-Si(OR)_3$.[9] An alkoxy group refers to a hydrocarbon that possesses a single bond to an oxygen atom. Thus, alkoxy groups are denoted simply as –OR. Our reading of patent[76-77] and open[9,71] literature as well as of product descriptions and specifications suggests that iPads® are currently coated by this chemistry using PFPE-$Si(OR)_3$. Thus, each PFPE chain is tethered to the glass substrate by only three Si-O-Si bonds at the most.

Not surprisingly, the coatings on iPads® are not durable. The mechanical stability of a grafted PFPE layer has been found to be greater for $(RO)_3Si$-PFPE-$Si(OR)_3$ when each PFPE chain is grafted by two sandwiching $-Si(OR_3)_3$ groups over that observed for a singly grafted PFPE-$Si(OR)_3$ chain.[78]

In principle, the mechanical stability of a grafted fluorinated layer can also be improved by using diblock copolymers FL_n-*b*-GX_m that consist of a fluorinated block of *n* FL units and a grafting/crosslinking block of *m* GX units. In comparison with the one trialkoxyl silane group found in PFPE-$Si(OR)_3$, a GX block incorporating many anchoring units should graft more readily to the substrate. Furthermore, an anchored layer made of a GX block is more stable than a layer derived from $-Si(OR)_3$. These anchored layers can produce polymer brushes that have many advantages over materials produced through other surface modification methods because of their mechanical and chemical robustness. In addition, they have a high degree of synthetic flexibility towards the introduction of many functional groups.[79-80]

Thus, reported in this thesis is the preparation of FL_n-*b*-GX_m brush layers that were applied as coatings onto glass plates. These fluorinated coatings provided the glass plates with self-cleaning properties. In addition, a systematic study was conducted to determine the factors affecting the preparation and properties of the coatings.

1.5 Introduction to Polymer Brushes

The desire to prepare functional polymer brushes has recently been of great interest due to their practical applications that are beneficial for our everyday life. Applications of these polymer brushes range from stabilizing pigment particles in paint, to cell adhesion, drug release, chemical sensing, stimuli responsive surfaces, and water- and oil- repellent coatings.[9,81-82,83-89] Due to their wide range of applications, these materials thus have great potential to improve our quality of life.

A polymer brush consists of long-chain polymer molecules that are fastened at one end to an interface or substrate.[90-91] The fastened ends of the polymer chains are sufficiently dense, that they experience crowding such that the polymer chains are forced to stretch away from the substrate or interface in an effort to avoid any overlap with each other.[92] Static repulsions and osmotic forces between the chains keep them from overlapping, which explains why polymer brushes are so useful in paint formulations.[93] This particular situation, where the fastened polymer chains are stretched away normal to the substrate, is quite different from the distinctive behaviour of a flexible polymer chain in solution where the chains adopt a random-walk configuration.[94] Much work in this field has shown that the deformation of densely fastened chains affects many aspects of their behavior and results in different novel properties of polymer brushes.[95] Some examples of other polymeric systems consisting of polymer brushes include polymer micelles, block copolymers at fluid-fluid interfaces, end-grafted polymers on solid surfaces and adsorbed diblock copolymers on solid surfaces.[93] All of these examples exhibit polymer chain deformations that can be seen in Figure 1-7.

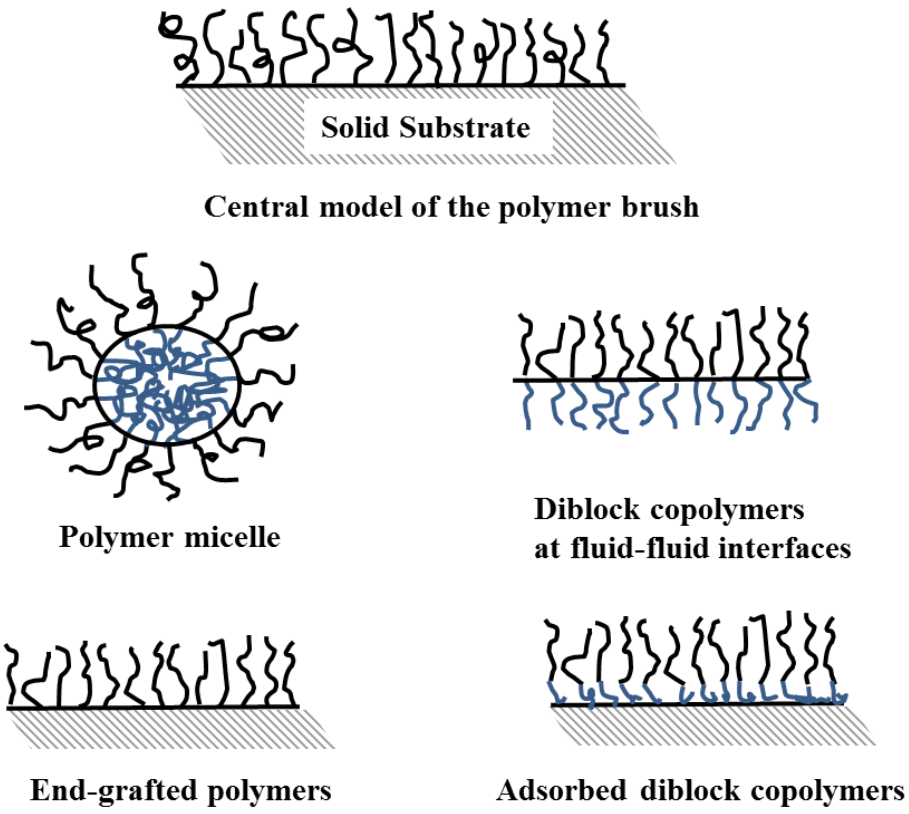

Figure 1-7 Examples of polymer systems containing polymer brushes.[93]

The tethering of polymer chains onto a surface or interface can be performed in a reversible or irreversible manner. On a solid surface, the chains can be physically adsorbed with "sticky" segments through physisorption,[96-97] or they can be chemically or covalently grafted. Physisorption onto a solid surface is typically accomplished with diblock copolymers where one block has a strong interaction with the substrate, while the other block has a rather weak interaction.[98] Fytas *et al.*[99] investigated the properties of a polystyrene-*block*-poly(ethylene oxide) (PS-b-PEO) diblock copolymer that was adsorbed onto a glass substrate to form a PEO anchor and a PS buoy. They used toluene as a good solvent for both blocks. It was found that the polar PEO blocks exhibited a stronger attraction to the surface than the nonpolar PS blocks, resulting in a brush formation by the stretched PS blocks. However, relying on this method can result in surfaces that are quite unstable especially when high shear forces are involved. In

addition, these kinds of surfaces can exhibit thermal and solvolytic instability due to the weak interaction between the substrate and the diblock copolymer making it a reversible process.[80,100]

Covalent attachment of polymer brushes can be obtained through 'grafting-to'[101-102] and 'grafting-from'[103-104] approaches. Such binding occurs when polymer chains are grafted onto substrates via chemical bond formation between reactive groups on the surface and the reactive endgroups of the chain.[79] Covalent attachment is more desirable than physisorption because it is an irreversible process. The 'grafting-to' approach refers to preformed end-functionalized polymers that react with an appropriate substrate to form a fastened polymer brush. Bergbreiter *et al.*[105] attached terminally functionalized poly(*tert*-butyl acrylate) chains onto oxidized polyethylene films through this method. Similarly, Ebata *et al.*,[106] grafted polysilane chains onto quartz surfaces and characterized these systems via UV-Vis spectroscopy. The covalent bond that forms between the substrate and the polymer chain imparts the polymer brush with chemical robustness which allows such coatings to be stable in harsh environments, such as exposure to dramatic temperature changes and to radiation.[107] This approach is quite simple, but it has some disadvantages. For example, it is limited to the preparation of polymer brushes with low grafting densities, as well as to thin films (films with thicknesses > 100 nm are inaccessible) due to the steric crowding of the reactive sites by already adsorbed polymers on the surface.[79]

To avoid these issues encountered with the 'grafting-to' method, researchers have turned to the 'grafting-from' approach instead. This methodology, often referred to as surface-initiated polymerization (SIP), involves the treatment of a surface to produce immobilized initiators. These initiators subsequently participate in an *in situ* surface initiated polymerization reaction. Many kinds of polymerization methods have been employed, but atom transfer radical polymerization (ATRP) is the most commonly utilized approach.[79] For example, Boven *et al.*[108] treated glass and silicon substrates with 3-aminopropyltriethoxysilane or (γ-APS), to produce amino functional groups on the surface. The azo initiators were then immobilized onto the surface through the formation of amide bonds between the γ-APS modified surface and an acid chloride functionalized azo initiator. Subsequent surface-initiated

radical polymerization reactions yielded PMMA chains that were fastened onto glass and silicon substrates. The 'grafting-from' approach has attracted significant interest due to its ability to provide polymer brushes with tunable grafting density, thickness and polydispersities from a large variety of monomers.[109] However, many steps are involved in these processes, which can become quite cumbersome. Therefore, for the purpose of this work, a 'grafting-to' approach has been employed as it is a simple technique. In addition, this approach was capable of providing the thin films (~12 nm) that were targeted for this investigation.

While there have been only a few reports describing grafted or crosslinked diblock copolymer brushes that were bound to solid substrates, diblock copolymer brushes that are physically deposited from selectively poor solvents for the anchoring block have been widely investigated.[110-112] Specifically, diblock copolymer brushes can be formed in block selective solvents that are good for one block but not the other (Figure 1-8) have drawn significant attention.[95,111,113] If the Gibbs free energy change associated with the chain rearrangement from the solution phase to the brush layer phase is negative, then the insoluble block will spread out and behave as a melt on the substrate, while the soluble block will stretch out in a similar manner as the bristles of a brush.[114] A negative Gibbs free energy is encouraged by a favorable interaction between the substrate and the insoluble block. This basic concept can help explain other diverse polymer systems such as polymeric surfactants, stabilized colloidal particles, and the various structures formed by block copolymers.[91]

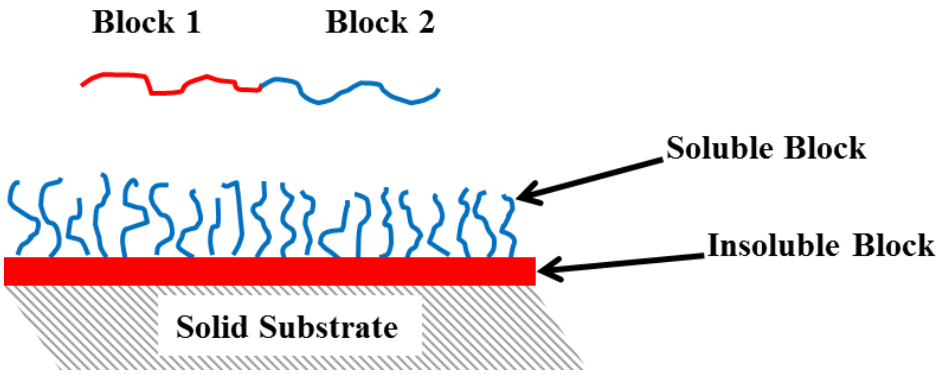

Figure 1-8 A graphic representation of a diblock copolymer forming a polymer brush in a block selective solvent. The insoluble block acts as a melt, while the soluble block reaches out into space in a similar manner as the bristles of a brush.

In this work, a 'grafting-to' approach was performed to covalently graft and crosslink P1-1, P1-2, and P2 diblock copolymers onto glass substrates. The reactive end-groups of the trialkoxysilane, or PIPSMA anchoring block underwent hydrolysis and polycondensation reactions to form Si-OH groups and Si-O-Si bonds with the preformed Si-OH groups on the glass substrate. The copolymers were deposited as thin brush layers by using a block selective solvent that preferred the overlying fluorinated block rather than the anchoring PIPSMA block. An excess amount of fluorinated solvent was present to ensure that the solution was selective for the overlying PFOEMA and PFPO blocks in each family of diblock copolymers. In this case, these blocks stretched out into solution to maximize their interaction with the fluorinated solvent molecules, thus creating a thin brush layer.

1.6 The Sol-gel Process

1.6.1 General Introduction

The sol-gel process involves the transformation of monomers into a colloidal solution (or sol), which acts as a precursor to an integrated network (or gel) of either discrete particles, or network polymers.[115-116] The sol gradually progresses towards the formation of a gel-like network consisting of both a liquid phase and a solid phase. Typical precursors for this process are metal alkoxides and metal

chlorides that undergo simultaneous hydrolysis (water consuming) and polycondensation (water forming) reactions to form polymeric species comprised of metal-oxygen-metal, or M-O-M bonds.[1] Tetraethyl orthosilicate (TEOS) is a widely used precursor due to its ability to undergo hydrolysis readily when exposed to water.[117] The many alkoxy groups attached to the silicon atom make it, and many others like it, popular choices as crosslinkers and coupling agents to produce glassy and ceramic materials.[118-119] Many researchers have also investigated the rates of these reactions, especially with the help of an acid or a base catalyst.[1,120]

The sol-gel process is a highly desirable technique, as it is relatively inexpensive, and produces surfaces with adequate homogeneity and respectable optical properties. It is also capable of coating large surface areas. The sol–gel process is especially efficient in producing thin, transparent, multi-component oxide layers of many compositions on a number of substrates, including glass.[121]

1.6.2 Sol-gel Hydrolysis and Condensation Reactions

As mentioned above, the sol-gel process involves the simultaneous hydrolysis and condensation of metal alkoxide precursors to form polymeric systems consisting of M-O-M bonds. Using silicon as an example, there are generally three main reactions to describe the sol-gel process as shown in Figure 1-9. Hydrolysis refers to the cleavage of chemical bonds by the addition of water, while condensation refers to the formation of bonds by the removal of water or an alcohol.[122] In reaction (1), hydrolysis occurs as a result of the nucleophilic attack of the oxygen contained in the water molecule, on the silicon atom.[117] Water is required to cleave the alkoxy groups off of the alkoxysilane, and produce Si-OH groups in their place. In addition to water, hydrolysis is also enabled in the presence of homogenizing agents such as alcohols, dioxane, THF, and acetone. However, this process is most rapid when catalysts are active in the system.[117]

According to reactions (2) and (3), polymerization to form Si-O-Si bonds occurs by either an alcohol producing (2), or a water producing (3) condensation reaction.[119] In these reactions, the newly produced Si-OH groups can react with other alkoxysilanes or with other Si-OH groups, respectively. Although it is possible for the condensation of Si-OH groups to proceed thermally without the aid of catalysts, their use is often necessary.[1]

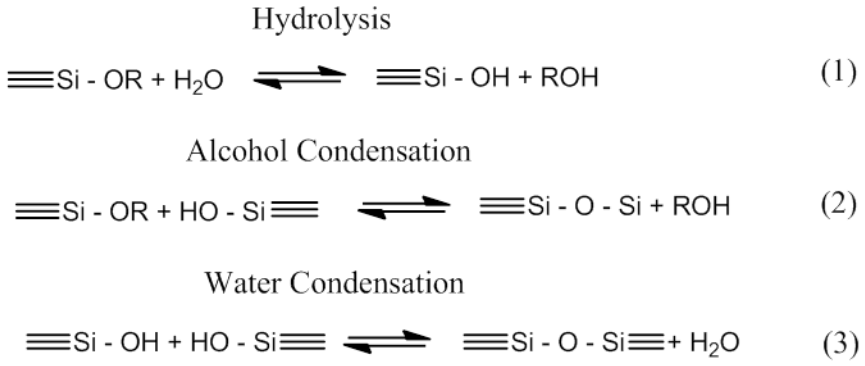

Figure 1-9 General reactions (1-3) describing the sol-gel process.[119]

1.6.3 Catalytic Effects on the Rate of the Sol-gel Process

It is possible for hydrolysis and condensation reactions to proceed without any aid from other chemical additives. However, there have been numerous reports indicating that the inclusion of catalysts will typically increase the rates of these reactions.[120,123] Mineral acids such as HCl and ammonia are generally used as additives for sol-gel processes.[117] The rate constants of the reactions in the sol-gel process are highly dependent upon the pH of the solution.[1] As the acid concentration in the system increases (causing the pH to decrease below 7), the rate constant also increases. In addition, as the base concentration in the system increases (causing the pH to increase above 7), the rate constant also increases. Pohl and Osterholtz[124] reported this trend when they obtained rate constants for γ-glycidoxypropyltrialkoxysilane in an aqueous solution as the pH in the system was varied between 5 and 9. Hence, reactions involving alkoxysilanes can be either acid or base catalyzed. Under acidic conditions,

trends in the literature suggest that branched "polymeric" networks are most preferably formed, whereas more discrete particle-like morphologies are formed under basic conditions.[1] Therefore, for the sake of this work, an acid catalyst was chosen to form a GX siloxane network in an acidic system.

Under acidic conditions, the hydrolysis reaction proceeds much more rapidly than the condensation reactions. During hydrolysis, the oxygen on the alkoxo group is protonated from the acid to create an alcohol, which provides a better leaving group. The oxygen from the water molecule then attacks the silicon atom to produce protonated $Si\text{-}O^{+}H_2$ groups. During the condensation reaction, neutral Si-OH groups attack the protonated $Si\text{-}O^{+}H_2$ groups to form Si-O-Si linkages and water as a byproduct.[1]

Herein this thesis, the diblock copolymers P1-1, P1-2, and P2 were covalently grafted and crosslinked onto glass surfaces to produce amphiphobic polymer brush layers. This brush layer was formed due to the block selective solvent that preferred the overlying fluorinated block, and through the sol-gel chemistry of the PIPSMA block. In the presence of an HCl catalyst, the PIPSMA block in each set of diblock copolymers underwent simultaneous hydrolysis and condensation reactions. This process is illustrated earlier in this chapter in Figure 1-2. During this procedure, the triisopropyl groups of the PIPSMA block were cleaved, to form Si-OH groups in their place. During the condensation reaction, the Si-OH groups reacted with other preformed Si-OH groups present on the surface of the glass, or with other Si-OH groups of the hydrolyzed polymer to form a network of Si-O-Si bonds. This process produced covalently grafted diblock copolymer chains covering glass surfaces that were optically clear and demonstrated amphiphobic and dynamic non-wetting properties.

1.7 Conclusions

This chapter has provided the background information that underlies the key concepts that are presented in this work. In particular, relevant information regarding water- and oil- repellent surfaces and the factors that affect their performance were discussed. In addition, the different fabrication methods to

produce such surfaces were described. Details about dynamic non-wetting surfaces and the factors that affect their performance were also provided. Additionally, the preparation and properties of polymer brushes, as well as an introduction to the sol-gel process taking place in this system was described in this chapter.

Chapter 2 will provide brief characterization details regarding the diblock copolymers P1-1/P1-2 and P2, as well as their use to prepare water- and oil- repellent surfaces on glass substrates. Furthermore, other characterization methods used during the course of this research including DRIFT-IR, AFM, XPS, UV-Vis, and various contact angle measurements (SCA, CAH, and SA) will also be discussed. Chapter 3 will pay emphasis on the results and discussion of the thesis that covers the factors that affect the performance of such amphiphobic surfaces. These factors that were varied included the catalyst amount, polymer amount, and block copolymer composition. Finally, Chapter 4 will provide a summary of this research and will propose potential future work of this project.

References

1. Brinker, C. J. *J. Non-Cryst. Solids* **1988,** *100*, 31-50.
2. Al-Hussein, M.; Serero, Y.; Konovalov, O.; Mourran, A.; Moller, M.; de Jeu, W. H. *Macromolecules* **2005,** *38*, 9610-9616.
3. Gao, Y.; Li, X. Y.; Hong, L. Z.; Liu, G. J. *Macromolecules* **2012,** *45*, 1321-1330.
4. Li, X. Y.; Gao, Y.; Xing, X. J.; Liu, G. J. *Macromolecules* **2013** *46*, 7436-7442.
5. Yarbrough, J. C.; Rolland, J. P.; DeSimone, J. M.; Callow, M. E.; Finlay, J. A.; Callow, J. A. *Macromolecules* **2006,** *39*, 2521-2528.
6. De Gennes, P.-G.; Brochard-Wyart, F.; Quéré, D. *Capillarity and Wetting Phenomena: Drops, Bubbles, Pearls, Waves*. Springer: New York, **2004**.
7. Erbil, H. Y. *Surface Chemistry: of Solid and Liquid Interfaces*. Wiley-Blackwell: Oxford, **2006**.
8. Ibach, H. *Physics of Surfaces and Interfaces*. Springer-Verlag: Berlin/Heidelberg, **2006**.
9. Cheng, D. F.; Masheder, B.; Urata, C.; Hozumi, A. *Langmuir* **2013,** *29*, 11322-11329.
10. Valipour M, N.; Birjandi, F. C.; Sargolzaei, J. *Colloids Surf., A* **2014,** *448*, 93-106.
11. Lam, C. N. C.; Wu, R.; Li, D.; Hair, M. L.; Neumann, A. W. *Adv. Colloid Interface Sci.* **2002,** *96*, 169-191.
12. Bhushan, B.; Jung, Y. C. *Prog. Mater. Sci.* **2011,** *56*, 1-108.
13. Rios, P. F.; Dodiuk, H.; Kenig, S.; McCarthy, S.; Dotan, A. *J. Adhes. Sci. Technol.* **2007,** *21*, 227-241.
14. Liu, K.; Tian, Y.; Jiang, L. *Prog. Mater. Sci.* **2013,** *58*, 503-564.
15. Hsieh, C.-T.; Chen, J.-M.; Kuo, R.-R.; Lin, T.-S.; Wu, C.-F. *Appl. Surf. Sci.* **2005,** *240*, 318-326.
16. McHale, G.; Shirtcliffe, N. J.; Aqil, S.; Perry, C. C.; Newton, M. I. *Phys. Rev. Lett.* **2004,** *93*, 036102.
17. Crone, T. J.; Tolstoy, M. *Science* **2010,** *330*, 634.
18. Nosonovsky, M.; Bhushan, B. *Curr. Opin. Colloid Interface Sci.* **2009,** *14*, 270-280.
19. Liu, K.; Yao, X.; Jiang, L. *Chem. Soc. Rev.* **2010,** *39*, 3240-3255.
20. Jin, X.; Yang, S.; Li, Z.; Liu, K.; Jiang, L. *Sci. China Chem.* **2012,** *55*, 2327-2333.
21. Rothstein, J. P. *Annu. Rev. Fluid Mech.* **2010,** *42*, 89-109.
22. Aulin, C.; Yun, S. H.; Wågberg, L.; Lindström, T. *ACS Appl. Mater. Interfaces* **2009,** *1*, 2443-2452.
23. Tuteja, A.; Choi, W.; Ma, M.; Mabry, J. M.; Mazzella, S. A.; Rutledge, G. C.; McKinley, G. H.; Cohen, R. E. *Science* **2007,** *318*, 1618-1622.
24. Paso, K.; Kompalla, T.; Aske, N.; R⊘nningsen, H. P.; Øye, G.; Sjöblom, J. *J. Dispersion Sci. Technol.* **2009,** *30*, 757-781.
25. Wang, D.; Wang, X.; Liu, X.; Zhou, F. *J. Phys. Chem. C* **2010,** *114*, 9938-9944.
26. Paso, K.; Viitala, T.; Aske, N.; Sjöblom, J. *Wax Deposition Prevention by Surface Modifications: Materials Evaluation*. Taylor & Francis: New York, **2012**.
27. Guo, Y.; Li, W.; Zhu, L.; Liu, H. *Mater. Lett.* **2012,** *72*, 125-127.
28. Xiong, D.; Liu, G.; Scott Duncan, E. J. *Polymer* **2013,** *54*, 3008-3016.
29. Andreas, S.; Zdenek, C.; Boris, F. S.; Manuel, S.; Wilhelm, B. *Bioinspiration Biomimetics* **2007,** *2*, S126.
30. Wang, C.; Yao, T.; Wu, J.; Ma, C.; Fan, Z.; Wang, Z.; Cheng, Y.; Lin, Q.; Yang, B. *ACS Appl. Mater. Interfaces* **2009,** *1*, 2613-2617.
31. Celia, E.; Darmanin, T.; Taffin de Givenchy, E.; Amigoni, S.; Guittard, F. *J. Colloid Interface Sci.* **2013,** *402*, 1-18.
32. Kota, A. K.; Choi, W.; Tuteja, A. *MRS Bull.* **2013,** *38*, 383-390.
33. Nagappan, S.; Park, S. S.; Yu, E. J.; Cho, H. J.; Park, J. J.; Lee, W.-K.; Ha, C.-S. *J. Mater. Chem. A* **2013,** *1*, 12144-12153.

34. Zhang, Z.; Zhu, X.; Yang, J.; Xu, X.; Men, X.; Zhou, X. *Appl. Phys. A* **2012,** *108*, 601-606.
35. Jin, C.; Jiang, Y.; Niu, T.; Huang, J. *J. Mater. Chem.* **2012,** *22*, 12562-12567.
36. Butt, H.-J.; Semprebon, C.; Papadopoulos, P.; Vollmer, D.; Brinkmann, M.; Ciccotti, M. *Soft Matter* **2013,** *9*, 418-428.
37. Feng, L.; Li, S.; Li, Y.; Li, H.; Zhang, L.; Zhai, J.; Song, Y.; Liu, B.; Jiang, L.; Zhu, D. *Adv. Mater.* **2002,** *14*, 1857-1860.
38. Zheng, Y.; Gao, X.; Jiang, L. *Soft Matter* **2007,** *3*, 178-182.
39. Yao, X.; Chen, Q.; Xu, L.; Li, Q.; Song, Y.; Gao, X.; Quéré, D.; Jiang, L. *Adv. Func. Mater.* **2010,** *20*, 656-662.
40. Liu, K.; Jiang, L. *Nano Today* **2011,** *6*, 155-175.
41. Liu, M.; Wang, S.; Wei, Z.; Song, Y.; Jiang, L. *Adv. Mater.* **2009,** *21*, 665-669.
42. Hikita, M.; Tanaka, K.; Nakamura, T.; Kajiyama, T.; Takahara, A. *Langmuir* **2005,** *21*, 7299-7302.
43. Young, T. *Phil. Trans. R. Soc. Lon.* **1805,** *95*, 65-87.
44. Xue, Z.; Liu, M.; Jiang, L. *J. Polym. Sci., Part B: Polym. Phys.* **2012,** *50*, 1209-1224.
45. Shibuichi, S.; Yamamoto, T.; Onda, T.; Tsujii, K. *J. Colloid Interface Sci.* **1998,** *208*, 287-294.
46. Tsujii, K.; Yamamoto, T.; Onda, T.; Shibuichi, S. *Angew. Chem. Int. Ed.* **1997,** *36*, 1011-1012.
47. Hirao, A.; Sugiyama, K.; Yokoyama, H. *Prog. Polym. Sci.* **2007,** *32*, 1393-1438.
48. Hare, E. F.; Shafrin, E. G.; Zisman, W. A. *J. Phys. Chem.* **1954,** *58*, 236-239.
49. Nishino, T.; Meguro, M.; Nakamae, K.; Matsushita, M.; Ueda, Y. *Langmuir* **1999,** *15*, 4321-4323.
50. Renner, R. *Environ. Sci. Technol.* **2006,** *40*, 12-13.
51. Campos, R.; Guenthner, A. J.; Haddad, T. S.; Mabry, J. M. *Langmuir* **2011,** *27*, 10206-10215.
52. Haynes, W. M. *CRC Handbook of Chemistry and Physics* 94th ed.; CRC Press: Taylor and Francis Group: Boca Raton, Florida, **2013**.
53. Wenzel, R. N. *J. Ind. Eng. Chem.* **1936,** *28*, 988-994.
54. Cassie, A. B. D.; Baxter, S. *Trans. Faraday Soc.* **1944,** *40*, 546-551.
55. Im, M.; Im, H.; Lee, J.-H.; Yoon, J.-B.; Choi, Y.-K. *Soft Matter* **2010,** *6*, 1401-1404.
56. Tuteja, A.; Choi, W.; McKinley, G. H.; Cohen, R. E.; Rubner, M. F. *MRS Bull.* **2008,** *33*, 752-758.
57. Tuteja, A.; Choi, W.; Ma, M. L.; Mabry, J. M.; Mazzella, S. A.; Rutledge, G. C.; McKinley, G. H.; Cohen, R. E. *Science* **2007,** *318*, 1618-1622.
58. Tuteja, A.; Choi, W. J.; McKinley, G. H.; Cohen, R. E.; Rubner, M. F. *MRS Bull.* **2008,** *33*, 752-758.
59. Deng, X.; Mammen, L.; Butt, H. J.; Vollmer, D. *Science* **2012,** *335*, 67-70.
60. Xiong, D. A.; Liu, G. J.; Zhang, J. G.; Duncan, S. *Chem. Mater.* **2011,** *23*, 2810-2820.
61. Xiong, D.; Liu, G. J.; Hong, L. Z.; Duncan, E. J. S. *Chem. Mater.* **2011,** *23*, 4357-4366.
62. Xiong, D. A.; Liu, G. J.; Duncan, E. J. S. *ACS Appl. Mater. & Interf.* **2012,** *4*, 2445-2454.
63. Jiang, W. J.; Grozea, C. M.; Shi, Z. Q.; Liu, G. J. *ACS Appl. Mater. & Interf.* **2013,** *6*, 2628-2637.
64. Xue, Z.; Liu, M.; Lei, J. *J. Polym. Sci., Part B: Polym. Phys.* **2012,** *50*, 1209-1224.
65. Nosonovsky, M.; Bhushan, B. *J. Phys. Condens. Matt.* **2008,** *20*.
66. Zhao, H.; Law, K. Y.; Sambhy, V. *Langmuir* **2011** *27*, 5927-5935.
67. Zhao, H.; Park, K. C.; Law, K. Y. *Langmuir* **2012,** *28*, 14925-14934.
68. Wong, T. S.; Kang, S. H.; Tang, S. K. Y.; Smythe, E. J.; Hatton, B. D.; Grinthal, A.; Aizenberg, J. *Nature* **2011,** *477*, 443-447.
69. Yao, X.; Dunn, S. S.; Kim, P.; Duffy, M.; Alvarenga, J.; Aizenberg, J. *Angew. Chem. Int. Ed.* **2014,** *53*, 4418-4422.
70. Wong, T.-S.; Kang, S. H.; Tang, S. K. Y.; Smythe, E. J.; Hatton, B. D.; Grinthal, A.; Aizenberg, J. *Nature* **2011,** *477*, 443-447.

71. Block, S.; Kleyer, D.; Hupfield, P.; Kitaura, E.; Itami, Y.; Masutani, T.; Nakai, Y. In *New Anti-Fingerprint Coatings*, 11th Annual Coatings for Plastics Symposium, Chicago, Paint & Coating Industry: Chicago, 2008; pp 88-92.
72. Cheng, D. F.; Urata, C.; Masheder, B.; Hozumi, A. *J. Am. Chem. Soc.* **2012,** *134*, 10191-10199.
73. Cheng, D. F.; Urata, C.; Yagihashi, M.; Hozumi, A. *Angew. Chem. Int. Ed.* **2012,** *51*, 2956-2959.
74. Furmidge, C. G. *J. Colloid Sci.* **1962,** *17*, 309-&.
75. Fadeev, A. Y.; McCarthy, T. J. *Langmuir* **1999,** *15*, 3759-3766.
76. Zieba, J.; Mayer, T. Anti-Moisture and Soil-Repellant Coatings. EU Patent 1702963 A1 2006.
77. Dams, R. J.; Fieuws, F. M.; Martin, S. J.; Terrazas, M. S.; Pellerite, M. J. Composition Comprising Fluorinated Polymether Silanes for Rendering Substrates Oil and Water Repellent. US Patent 6613860 B1 2003.
78. Kondo, H.; Sungkil, L.; Hanaoka, H. *Tribol. Lubr. Technol.* **2009,** *65*, 54-61.
79. Edmondson, S.; Osborne, V. L.; Huck, W. T. S. *Chem. Soc. Rev.* **2004,** *33*, 14-22.
80. Yu, B.; Zheng, Z.-J.; Li, Y.; Zhou, F. *J. Fiber Bioeng. Inform.* **2009,** *1*, 249-260.
81. Napper, D. H. *Polymeric Stabilization of Colloidal Dispersions*. Academic Press: London, **1983**.
82. Urata, C.; Masheder, B.; Cheng, D. F.; Hozumi, A. *Langmuir* **2013,** *29*, 12472-12482.
83. Takahashi, H.; Matsuzaka, N.; Nakayama, M.; Kikuchi, A.; Yamato, M.; Okano, T. *Biomacromolecules* **2011,** *13*, 253-260.
84. Raynor, J. E.; Petrie, T. A.; Fears, K. P.; Latour, R. A.; García, A. J.; Collard, D. M. *Biomacromolecules* **2009,** *10*, 748-755.
85. Harris, B. P.; Kutty, J. K.; Fritz, E. W.; Webb, C. K.; Burg, K. J. L.; Metters, A. T. *Langmuir* **2006,** *22*, 4467-4471.
86. Minko, S. *J. Macromol. Sci., Part C* **2006,** *46*, 397-420.
87. Abu-Lail, N. I.; Kaholek, M.; LaMattina, B.; Clark, R. L.; Zauscher, S. *Sens. Actuators, B* **2006,** *114*, 371-378.
88. Chen, T.; Ferris, R.; Zhang, J.; Ducker, R.; Zauscher, S. *Prog. Polym. Sci.* **2010,** *35*, 94-112.
89. Lue, S. J.; Hsu, J.-J.; Wei, T.-C. *J. Membr. Sci.* **2008,** *321*, 146-154.
90. Stuart, M. A. C.; Huck, W. T. S.; Genzer, J.; Müller, M.; Ober, C.; Stamm, M.; Sukhorukov, G. B.; Szleifer, I.; Tsukruk, V. V.; Urban, M.; Winnik, F.; Zauscher, S.; Luzinov, I.; Minko, S. *Nat. Mater.* **2010,** *9*, 101-113.
91. Milner, S. *Science* **1991,** *251*, 905-914.
92. Tu, H.; Heitzman, C. E.; Braun, P. V. *Langmuir* **2004,** *20*, 8313-8320.
93. Zhao, B.; Brittain, W. J. *Prog. Polym. Sci.* **2000,** *25*, 677-710.
94. Yamakawa, H. *Helical Wormlike Chains in Polymer Solutions*. Springer-Verlag GmbH: Berlin, **1997**.
95. Halperin, A.; Tirrell, M.; Lodge, T. P. *Adv. Polym. Sci.***1992,** *100*, 31-71.
96. Parsonage, E.; Tirrell, M.; Watanabe, H.; Nuzzo, R. G. *Macromolecules* **1991,** *24*, 1987-1995.
97. Kelley, T. W.; Schorr, P. A.; Johnson, K. D.; Tirrell, M.; Frisbie, C. D. *Macromolecules* **1998,** *31*, 4297-4300.
98. Bug, A. L. R.; Cates, M. E.; Safran, S. A.; Witten, T. A. *J. Chem. Phys.* **1987,** *87*, 1824-1833.
99. Fytas, G.; Anastasiadis, S. H.; Seghrouchni, R.; Vlassopoulos, D.; Li, J.; Factor, B. J.; Theobald, W.; Toprakcioglu, C. *Science* **1996,** *274*, 2041-2044.
100. Fleer, G. *Polymers at Interfaces*. Chapman and Hall: London, **1993**.
101. Draper, J.; Luzinov, I.; Minko, S.; Tokarev, I.; Stamm, M. *Langmuir* **2004,** *20*, 4064-4075.
102. Motornov, M.; Sheparovych, R.; Lupitskyy, R.; MacWilliams, E.; Hoy, O.; Luzinov, I.; Minko, S. *Adv. Funct. Mater.* **2007,** *17*, 2307-2314.
103. Ayres, N.; Cyrus, C. D.; Brittain, W. J. *Langmuir* **2007,** *23*, 3744-3749.
104. Azzaroni, O.; Brown, A. A.; Huck, W. T. S. *Angew. Chem. Int. Ed.* **2006,** *45*, 1770-1774.
105. Bergbreiter, D. E.; Franchina, J. G.; Kabza, K. *Macromolecules* **1999,** *32*, 4993-4998.
106. Ebata, K.; Furukawa, K.; Matsumoto, N. *J. Am. Chem. Soc.* **1998,** *120*, 7367-7368.

107. Jeon, N. L.; Choi, I. S.; Whitesides, G. M.; Kim, N. Y.; Laibinis, P. E.; Harada, Y.; Finnie, K. R.; Girolami, G. S.; Nuzzo, R. G. *Appl. Phys. Lett.* **1999,** *75*, 4201-4203.
108. Boven, G.; Folkersma, R.; Challa, G.; Schouten, A. J. *Polym. Commun.* **1991,** *32*, 50-53.
109. Prucker, O.; Rühe, J. *Macromolecules* **1998,** *31*, 592-601.
110. Tao, J.; Guo, A.; Liu, G. *Macromolecules* **1996,** *29*, 1618-1624.
111. Tao, J.; Guo, A.; Stewart, S.; Birss, V. I.; Liu, G. *Macromolecules* **1998,** *31*, 172-175.
112. Tao, J.; Liu, G. *Macromolecules* **1997,** *30*, 2408-2411.
113. Ding, J.; Liu, G. *Langmuir* **1999,** *15*, 1738-1747.
114. Ding, J.; Birss, V. I.; Liu, G. *Macromolecules* **1997,** *30*, 1442-1448.
115. Klein, L. C.; Garvey, G. J. *J. Non-Cryst. Solids* **1980,** *38–39, Part 1*, 45-50.
116. Brinker, C. J.; Keefer, K. D.; Schaefer, D. W.; Ashley, C. S. *J. Non-Cryst. Solids* **1982,** *48*, 47-64.
117. Vorankov, M. G.; Mileshkevich, V. P.; Yuzhelevski, Y. A. *The Siloxane Bond: Physical Properties and Chemical Transformations*. Consultants Bureau: New York, **1978**.
118. Plueddemann, E. P. *Silane Coupling Agents*. Springer: New York, **1982**.
119. Osterholtz, F. D.; Pohl, E. R. *J. Adhesion Sci. Technol.* **1992,** *6*, 127-149.
120. Pope, E. J. A.; Mackenzie, J. D. *J. Non-Cryst. Solids* **1986,** *87*, 185-198.
121. Ilican, S.; Caglar, Y.; Caglar, M.; Yakuphanoglu, F. *Appl. Surf. Sci.* **2008,** *255*, 2353-2359.
122. McNaught, A. D.; Wilkinson, A. *IUPAC. Compendium of Chemical Terminology*. 2nd ed.; Blackwell Scientific Publications: Oxford, **1997**.
123. Schmidt, H.; Scholze, H.; Kaiser, A. *J. Non-Cryst. Solids* **1984,** *63*, 1-11.
124. Pohl, E. R.; Osterholtz, F. D.; Ishida, H.; Kumar, G. *Molecular Characterization of Composite Interfaces*. Plenum Press: New York **1985**.

Chapter 2

Experimental Details

2.1 Introduction

This thesis describes a facile approach for the development of amphiphobic surfaces that are smooth, thin and optically clear on glass plates. The diblock copolymers P1-1, P1-2, and P2 were synthesized via atom transfer radical polymerization (ATRP), before they were individually dissolved in a good solvent to yield polymer solutions that were subsequently deposited onto glass substrates. With the addition of an acid catalyst diluted in a solvent that was selective for the anchoring block, a polymer brush was formed through the covalent grafting and crosslinking of the PIPSMA block onto the surface via sol-gel chemistry. During this process, simultaneous hydrolysis and condensation reactions occurred. The triisopropyl groups located on the PIPSMA block were cleaved, and formed silanol groups (Si-OH) that facilitate covalent attachment onto the substrate. As the condensations proceeded further, siloxane bonds (Si-O-Si) were formed between the produced Si-OH groups and other Si-OH groups present on the surface of the glass, or with other Si-OH groups of the hydrolyzed polymer. The solvent was slowly evaporated in a sealed container so that the Si-OH groups produced would have sufficient time to become grafted onto the glass plate, and the grafted copolymer chains would have enough time to organize into a brush layer. Upon evaporation, the fluorinated block extended outwardly like the bristles of a brush which rendered smooth, thin, and optically clear amphiphobic coatings that covered the glass plate.

This chapter describes the preparation of smooth amphiphobic coatings for glass plates using the diblock copolymers P1-1, P1-2 and P2. For the sake of comparison, the preparation of an additional coated plate using a PFOEMA homopolymer is also defined. The preparation of PIPSMA homopolymer samples in order to evaluate the rate of the sol-gel process is also described. In addition, CA measurements (SCA, CAH, and SA) that were performed to determine the static and dynamic de-wetting capabilities of those water- and oil- repellent films are discussed. Furthermore, the preparation of samples

for DRIFT-IR, AFM, XPS, UV-Vis, as well as for durability and anti-smudge characterization through these techniques are also described in this chapter.

2.2 Materials

The P1-1 and P1-2 diblock copolymers were synthesized via ATRP. This polymerization technique was also used to prepare the PIPSMA block of P2. The PFPO block of P2 was derived from Krytox157 FLS, which was purchased from DuPont. PIPSMA and PFOEMA homopolymers with 20 and 17 repeat units respectively, were both synthesized via ATRP and their respective number-average molecular weights were 6600 and 9000 g/mol. The synthesis and characterization of these polymers were conducted by Dr. Muhammad Rabnawaz of the Liu Group (Appendix). α,α,α-Trifluorotoluene (TFT, 99+%, Acros), tetrahydrofuran (THF, 99.9%, Fisher Scientific), sulfuric acid (H_2SO_4, 18 M, Fisher), and hydrogen peroxide (H_2O_2, 30%, Fisher) were used as received. Hydrochloric acid (HCl, 13 M, Fisher) was diluted with THF prior to use.

2.3 Preparation of the Glass Coatings

Fisherbrand glass plates with a dimension of 1.0×1.3 cm^2 were cleaned using a Piranha solution (4/1 v/v concentrated H_2SO_4/30% H_2O_2). *Caution: Piranha solution is a very strong oxidant.* These glass plates were subsequently rinsed in water, methanol, and then dried under nitrogen gas before use. To coat a glass plate, it was initially placed in a weighing bottle (see Figure 2-1). TFT (62 μL), 1.0–3.0 μL of a diblock copolymer solution (at 1.0 mg/mL of P1-1, P1-2, or P2 in TFT), and 27 μL of an HCl solution dissolved in THF were sequentially dispensed onto the plate. The HCl solution was prepared by diluting an aqueous HCl solution (13 M) with THF to concentrations of 3.0×10^{-1} M, 3.0×10^{-2} M, 3.0×10^{-3} M, and 3.0×10^{-4} M depending on the desired solution acidity. The volume of the polymer coating solution

and the HCl concentration in THF were varied to examine the effect of changing the amounts of polymer, and the catalyst on the properties of the resultant coatings. The weighing bottle was then covered with its lid and ~ 19 h was allowed to elapse before the solvent evaporated. The exact amount of the polymer was adjusted according to the final glass plate area.

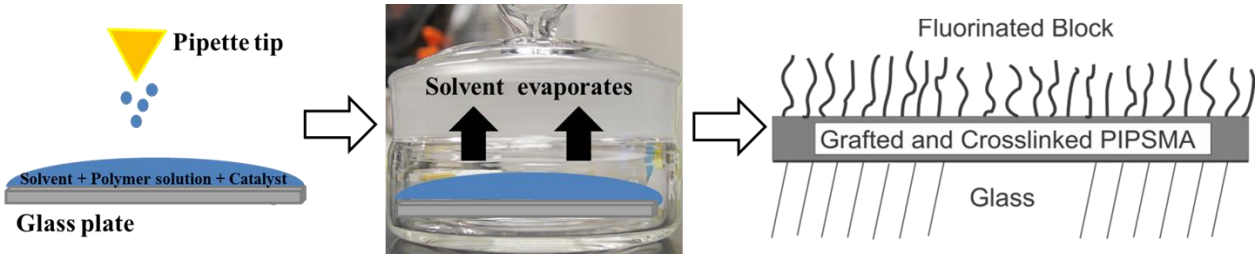

Figure 2-1 Schematic illustration of the coating procedure.

Detailed calculations for determining the thickness of the polymer films and theoretical polymer amounts are shown in the Appendix. For the P1-1/P1-2 coated plates, less than the theoretical amount of copolymer was used because through CA measurements it appeared that a saturated brush layer had already formed. Consequently, it was not necessary to add additional polymer. In the case of the P2-coated plates, an excess amount of copolymer was used to ensure that the plate was fully covered as shown in Table 2-1.

In one case, a thin PFOEMA coating was needed for XPS analysis. This coating was prepared by dispensing 62 µL of TFT onto a glass plate first and then adding 1.95 µL of a PFOEMA solution at 1.0 mg/mL in TFT. The solvent was then allowed to evaporate slowly from the weighing bottle.

Table 2-1 Amounts of diblock copolymer used to coat each type of glass plate.

Type of Coated Glass Plate	Theoretical Amount of Copolymer to Cover a Glass Plate (µg/cm^2)	Amount of Copolymer Used to Coat the Glass Plate (µg/cm^2)
P1-1	2.0	1.5
P1-2	2.2	1.9
P2	1.2	1.5

2.4 Preparation of PIPSMA Homopolymer Sol-gel Samples

Two 1.0 mL THF solutions containing 10.0 mg/mL of PIPSMA were prepared. To one of these solutions, 0.050 mL of an HCl solution in THF at 6.2×10^{-1} M was added, and to the other, 0.010 mL of an HCl solution at 1.0×10^{-3} M was added. 50 µL aliquots of these solution mixtures were collected before the catalyst was added, or at different times after the mixtures were prepared. These aliquots were directly added to 0.12 g of KBr that was previously ground in to a powder using a mortar and pestle. The components were mixed together with a plastic spatula, and the THF was left to evaporate out of the sample for 30 min to yield a dry powder for DRIFT-IR analysis.

2.5 CA Measurements

SCA, CAH, and SA measurements were performed at room temperature (21-23 ˚C) over the course of several days using deionized water, diiodomethane (>99%, Aldrich), and hexadecane (>99%, Aldrich). These were measured using a Dataphysics® OCA 15Pro optical contact angle measuring system equipped with a TBU 90E electronic tilting base. A Hamilton 500 µL syringe was used to dispense each of the probe liquids.

2.5.1 SCA Measurements

SCAs were measured by placing 5 µL droplets of the different probe liquids onto three different areas of the glass plate. These measurements were performed with the Dataphysics® system set to the "sessile drop" mode. The reported SCA represented an average of three different measurements.

2.5.2 CAH Measurements

In this work, the CAH was calculated as the difference between the cosine of the θ_{rec} and θ_{adv} CAs.[1] The θ_{adv} and θ_{rec} CAs were defined as the largest and smallest angles possible without increasing or decreasing the droplet's solid/liquid interfacial area respectively.[2-3] In this work, two different methods were performed to define the CAH of each prepared surface as described by the Dataphysics® software. These methods included the automatic advancing and receding contact angle (ARCA) method, and the tilting drop (TD) method.[4] With the use of both of these approaches, a very similar θ_{adv} was obtained for all of the liquids tested. However, a different θ_{rec} was obtained for the oil liquids even at lower withdrawing speeds of 0.1 µL/s. θ_{rec} values measured from the ARCA method should be less accurate because the needle attached to a droplet undergoing size changes should have somewhat perturbed the shape of the droplet.[5] Hence, the ARCA method was used only for water, and the TD method, that involved the use of free-standing liquid droplets, was used for the measurement of the θ_{rec} of the oil droplets.

In the ARCA approach, each measurement was conducted by initially dispensing a 5 µL droplet of water onto the surface using the "sessile drop needle-in" mode on the measuring system. The SCA was initially obtained to ensure that both the left and right angles of the droplet were as similar as possible for accurate results. The Dataphysics® software began tracking the SCA over time, and displayed a graph of the CA vs. the run number to show the stability of the droplet before the ARCA experiment was initialized. In this case, the run number referred to a particular instant when a measurement was taken by the instrument. During the ARCA cycle, an extra 5 µL of the probe liquid was added to the droplet to find θ_{adv}, followed by the subtraction of 5 µL to determine θ_{rec}. This was performed at a rate of 0.5 µL/s with a delay time of 2 s between each liquid addition and withdrawal step. As the size of the liquid droplets changed, both the CA and droplet base diameter (mm) were recorded to define θ_{adv} and θ_{rec}. This was performed by plotting a graph of the droplet base diameter vs. the run number. Instead of recording θ_{adv} and θ_{rec} at one particular instant before the droplet interfacial area changed, a range of values were

selected to calculate the mean θ_{adv} and θ_{rec} values to account for experimental error. The θ_{adv} values were selected starting from immediately before the droplet base diameter increased, to when the base diameter plateaued. Similarly, the θ_{rec} values were selected starting from just before the base diameter decreased, to when the base diameter reached a plateau. The selected ranges of base diameter values corresponded to the appropriate ranges of the SCA values measured during the process. The mean values of the two corresponding SCA ranges were recorded as θ_{adv} and θ_{rec}, respectively. An example of a set of data obtained using this approach can be seen in Figure 2-2.

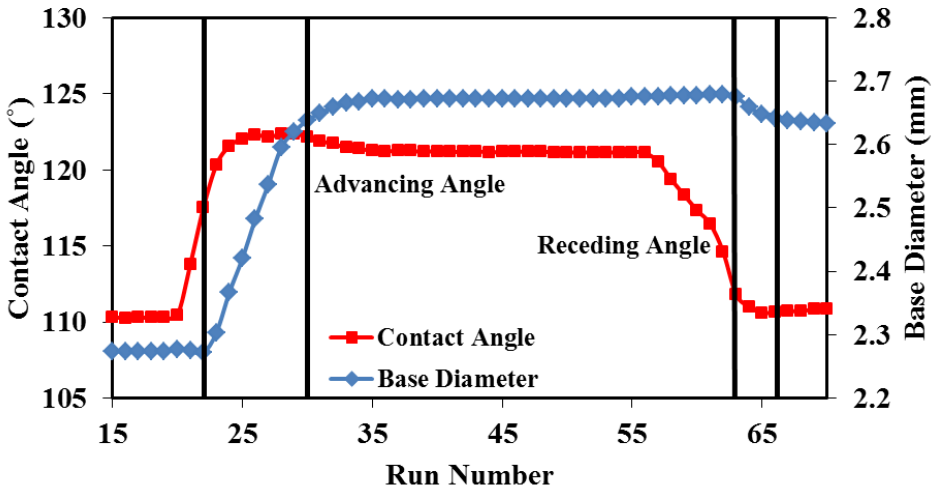

Figure 2-2 A plot showing the change in a water droplet's base diameter and CA as 5 µL of water is both added to and removed from the droplet sitting on a P1-2 coated glass plate at an HCl concentration of 0.90×10^{-1} M. The mean θ_{adv} and θ_{rec} angles were determined by taking the average of the base diameter set of values (shown in blue) seen between the two sets of black lines, and matching them with the appropriate CA set of values (shown in red).

In the TD approach, 5 µL oil droplets were deposited onto the glass surface in the "sessile drop" mode. The initial SCA and droplet base diameter data was obtained for the droplet. The TBU 90E tilting base unit was initiated, and began tilting the glass plate at a rate of 0.37˚/s as shown in Figure 2-3. This tilting process was interrupted every 0.2˚ to re-measure both the SCA (right and left side) and the base diameter of the droplet. The mean θ_{adv} (right) and θ_{rec} (left) angles were recorded when the constant droplet base diameter "slipped" to produce a change in the solid/liquid interfacial area. The "slip" motion

referred to the instant when the deformed droplet moved to release the built up liquid force on the solid substrate.

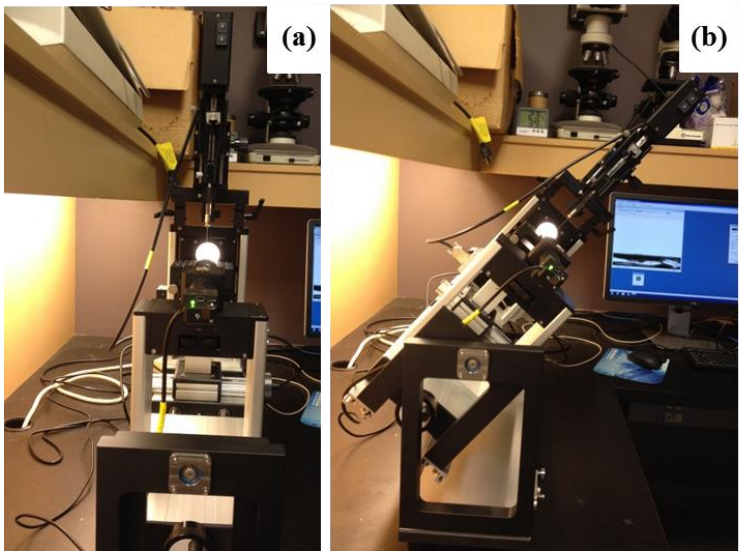

Figure 2-3 Optical images of the OCA 15Pro contact angle instrument equipped with a TBU 90E tilting base before (a) and after (b) the measurements were recorded.

2.5.3 SA Measurements

In this work, the SA was measured as the angle at which a droplet placed on a substrate would completely roll off a surface. These measurements were conducted by dispensing the probe liquid onto the surface of the substrate, and tilting the substrate at greater angles using an electronic TBU 90E tilting base unit (a component of the Dataphysics® OCA 15Pro system) as shown above at a rate of 0.37˚/s. This tilting angle was increased until the liquid droplet completely rolled off the surface. These measurements were conducted using 20.0 µL droplets at three different positions on each sample.

2.6 Characterization Methods

2.6.1 Diffuse-Reflectance Infrared Fourier-Transform Spectroscopy (DRIFT-IR)

The DRIFT-IR spectra of the sol-gel PIPSMA homopolymer samples were recorded at 0 min, 30 min, and 21 h, and at 0 min and 2 h, for the 6.2×10^{-1} M and 1.0×10^{-3} M samples, respectively. These measurements were recorded using a Varian 640-IR and a Varian Scimitar 1000 FT-IR spectrometer.

2.6.2 Atomic Force Microscopy (AFM)

AFM height and phase images of the coated films were obtained using a Veeco Multimode instrument equipped with a Nanoscope IIIa controller that was operated in the Tapping Mode. Rectangular-shaped silicon probes (AppNano, ACT) with a 300 kHz resonance frequency and a spring constant of 40 N/m were used. All plates that were imaged were freshly prepared immediately after evaporation.

2.6.3 X-ray Photoelectron Spectroscopy (XPS)

XPS measurements of P1-1, P1-2, and P2 were performed using a Thermo Instruments Microlab 310F surface analysis system that was equipped with an Mg Kα X-ray source (1253.6 eV). An anode potential of 15 kV and an emission current of 20 mA was used. Spectra were acquired in the fixed analyzer transmission mode with a pass energy of 20 eV and a surface/detector takeoff angle of 20°. All spectra were calibrated to the C1s line located at 285.0 eV.

2.6.4 Ultraviolet-Visible Spectroscopy (UV-Vis)

The UV-Vis transmittance spectra of clean uncoated glass plates and glass plates coated with P1-1, P1-2 and P2 were recorded using a Perkin Elmer Lambda XLS+ spectrometer. The plates were simply placed in front of the beam and the measurement was recorded.

2.6.5 Durability and Anti-Smudge Measurements

In order to determine whether the PIPSMA block was indeed covalently grafted onto the surface, the plates were submerged into 2 mL of TFT. This solution was stirred overnight at 200 rpm to remove any polymer that had become physically deposited onto the surface. After this process, the water CA was then re-measured.

The anti-smudge properties and mechanical durability of the coated glass plates were tested using a permanent black marker (Sharpie®) and a homemade mechanical device. The marker was used to write on the coated glass plates, and the plates were subsequently rubbed with a light-duty tissue wiper (VWR). This process of writing on and subsequently rubbing the plates was repeated ten times. The SCAs were then re-measured. The homemade mechanical device (Figure 2-4) used in determining the film stability was equipped with a cotton covered probe that was located at the bottom of a rotating shaft, which rotated at 40 rpm with 500 g of applied force on each coated surface. The adjustable jack was raised or lowered to press or release the cotton probe on and off the stage, respectively. Hidden springs located on the inside walls of the device allowed the stage to be moved up and down, enabling the force to be adjusted appropriately. Initial water SCA measurements were taken before the process began. Durability measurements were recorded at 1 min, 5 min, and 1 h after the process began, and the water SCA was subsequently re-measured.

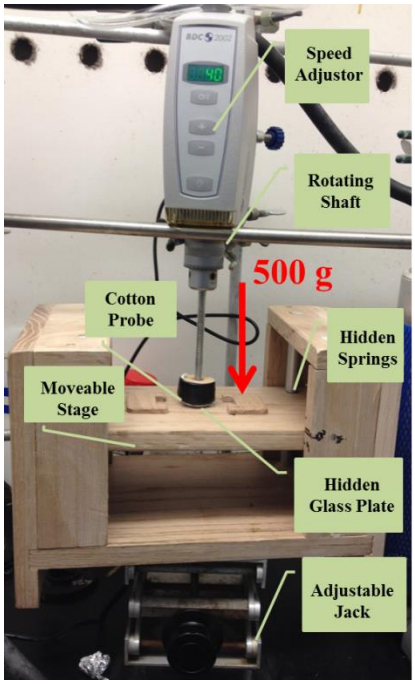

Figure 2-4 Photograph of the homemade mechanical device used to evaluate the durability of the coatings.

References

1. Cheng, D. F.; Masheder, B.; Urata, C.; Hozumi, A. *Langmuir* **2013,** *29*, 11322-11329.
2. Lam, C. N. C.; Wu, R.; Li, D.; Hair, M. L.; Neumann, A. W. *Adv. Colloid Interface Sci.* **2002,** *96*, 169-191.
3. He, B.; Lee, J.; Patankar, N. A. *Colloids Surf., A* **2004,** *248*, 101-104.
4. Gerhard, M.; Norbert, H. *Datsphysics Operating Manual OCA 15Pro Video Based Optical Contact Angle Measuring Instrument*. Dataphysics Instruments GmbH: Filderstadt, Germany, **2013**.
5. Erbil, H. Y.; McHale, G.; Rowan, S. M.; Newton, M. I. *Langmuir* **1999,** *15*, 7378-7385.

Chapter 3

Results and Discussion

3.1 Introduction

As mentioned in Chapter 1, a surface that can repel both water and oil at a CA > 90˚ is considered to be amphiphobic.[1] Surfaces on which water and oil droplets possess CAs that may be less than 90˚ but readily slide off are dynamically non-wetting amphiphobic surfaces. Amphiphobic surfaces have excellent self-cleaning, anti-fouling, corrosion resistant, and anti-bacterial properties.[2-8] Because of their dual repellency, amphiphobic coatings are more difficult to prepare than standard hydrophobic coatings.[9] However, these coatings are desirable for protecting metal surfaces against corrosion,[10] shielding the walls of buildings from graffiti,[11-12] protecting electronic hand-held devices against spills or fingerprints[13-15] as well as for various other applications. On a smooth surface with no added roughness, it has been shown that the chemical composition of the material is of high importance.[14] A low surface free energy is a critical feature of self- cleaning surfaces, and this property will improve the amphiphobicity of a material.[16] For this reason, perfluoroalkylsilanes or other fluorosilane-containing compounds are commonly used to produce amphiphobic coatings[17] because their CF_3 groups may pack hexagonally and closely to yield surfaces with a surface free energy as low as 6.7 mN/m,[18-20] which is currently the lowest reported value.[12] Other advantages provided by fluoropolymers include their good chemical/thermal stability and low friction coefficients.[19] Silanes can also readily undergo covalent attachment to mineral substrates such as mica, glass and metal-oxide surfaces due to their many hydroxyl groups,[21] which can form Si-O-Si bonds to produce a coating network.

Although having smooth amphiphobic surfaces that can achieve high water and oil SCAs are highly desireable, these properties alone are simply not sufficient for many applications.[22] More interest revolves around the dynamic de-wetting capabilities of such coatings (such as the sliding behavior), and how to render these materials “anti-smudge” and “fingerprint-resistant”. A recent example of an anti-

smudge coating prepared by Muthiah *et al*[13,23] required a complex dual-layered coating based on fluorobinders and silica nanoparticles. The usage of nanoparticles can enhance the amphiphobic properties of a coating, but it comes at a cost to a coating's roughness, transparency, and mechanical durability.[24] More practical approaches to produce smooth and transparent amphiphobic coatings on glass have been developed by the Hozumi group.[22,25] They used perfluoroalkylsilanes or trimethoxysilyl-terminated perfluorinated polyethers that can react with the Si-OH groups on glass substrates. Furthermore, they improved the wettability properties of their coatings by incorporating tetramethoxysilane molecules. Toselli *et al*.[26] also used a commercial triethoxysilane terminated perfluoropolyether with a T_g of -120˚ to prepare organic-inorganic hybrid surfaces with dual repellency. However, a perfluoroalkylsilane layer grafted by one terminal trialkoxysilane group may be less stable than a diblock copolymer-based layer due to a lower number of siloxane bonds used for attachment to a glass surface. In addition, a diblock copolymer-based coating would be thicker, and thus have greater resistance against detachment and penetration by etchants.[27]

In this thesis, I present a facile approach for the preparation of smooth, thin-film amphiphobic coatings with anti-smudge and dynamic non-wetting properties based on the fluorinated diblock copolymers PIPSMA-*b*-PFOEMA (P1-1/P1-2) and PFPO-*b*-PIPSMA (P2). A schematic diagram depicting the coating process can be seen in Figure 3-1 using P1-1/P1-2 as an example. This strategy involved preparing two types of polymer brushes by dissolving each diblock copolymer in a solution of TFT, which was a good solvent for both blocks. The polymer solution was then dispensed onto a glass plate. Upon addition of a dilute acid catalyst in THF, the triisopropyl groups in each case were cleaved via sol-gel reaction processes and the binding block became less soluble in the solvent.[28-29] This block would tend to deposit on the plate. Through simultaneous hydrolysis and condensation reactions, Si-OH groups formed that were capable of grafting onto the glass substrate as well as with other PIPSMA blocks. As the condensation reactions proceeded further, Si-O-Si bonds formed to create an anchored crosslinked layer covering the substrate. Since THF has a lower boiling point (65 ˚C) than TFT (102 ˚C),[30] the THF would

evaporate faster from the system leaving an excess of TFT, which was selective for the overlying fluorinated blocks. Upon slow evaporation, the fluorinated blocks would extend outwardly into the solution, which would render the coating with amphiphobic properties.

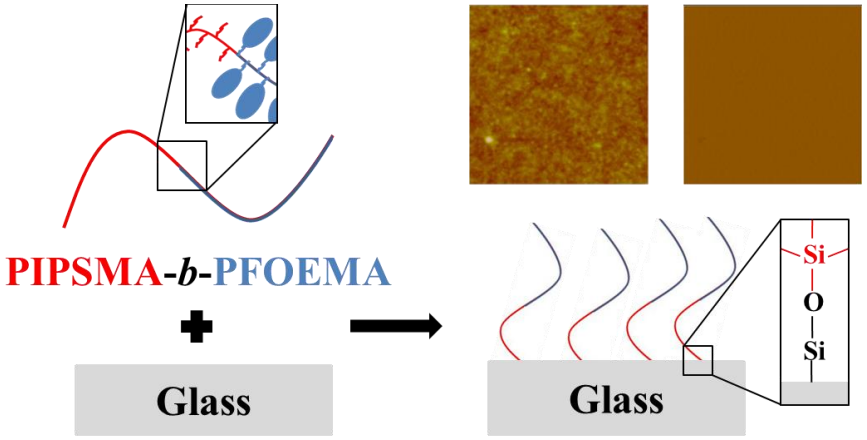

Figure 3-1 Schematic diagram depicting the procedure used to prepare the polymer brush amphiphobic coatings using P1-1/P1-2 as an example. The inset shows 2.0 × 2.0 μm^2 height and phase AFM images (on the left and right respectively) of a coated glass plate.

3.2 Diblock Copolymers

All diblock copolymers used and referred to in this work, were both synthesized and characterized by Dr. Muhammad Rabnawaz of the Liu Group. The properties of the diblock copolymers are summarized in Table 3-1 below.

Table 3-1 Characteristics of the diblock copolymers used.

Sample	M_n (g/mol)[a]	M_w/M_n[a]	n[b]	m[b]
P1-1	17600	1.14	18	22
P1-2	19400	1.12	13	30
P2	4500	1.10	14	7

[a] Determined via SEC characterization. [b] Determined by ^{1}H NMR spectroscopy.

3.3 Coating of the Glass

In order to coat a glass plate of an area of ~1.3 cm^2, the plate was initially held level inside a weighing bottle. Sequentially, 62-μL of TFT and 1 – 3 μL of a diblock copolymer solution (1.0 mg/mL in TFT) were dispensed onto the plate. HCl was also added to trigger the sol-gel chemistry of the PIPSMA block of P1-1, P1-2, or P2. Subsequently, the lid was placed onto the weighing bottle to slow down solvent evaporation. This was done to ensure that the formed Si-OH groups had sufficient time to graft onto the glass plate, and that the grafted copolymer chains had enough time to organize into a brush layer.

3.4 Effect of Varying the HCl Concentration on the Coating Properties

To investigate the effect of varying the HCl concentration on the sol-gel chemistry of the PIPSMA block of the copolymers, a PIPSMA homopolymer was initially examined as a model system. PIPSMA was treated in THF at different HCl concentrations, and samples were collected at different times and dried for compositional analysis via diffuse reflectance Fourier-transform infrared (DRIFT-IR) spectroscopy. At an HCl concentration of 6.2×10^{-1} M, the DRIFT-IR analysis indicated that a strong peak at 3351 cm^{-1} corresponding to Si-OH groups[31] was observed within 30 min. The appearance of this signal suggested that significant triisopropyloxysilane hydrolysis had occurred during this time period (Figure 3-2a). At 21 h, a strong absorption peak at 1069 cm^{-1} corresponding to Si-O-Si stretching appeared, suggesting the occurrence of the expected gelation or Si-OH condensation. However, neither Si-OH nor Si-O-Si absorption bands were noticeable in the dried reacted mixture 2 h after HCl was added to a concentration of 1.0×10^{-3} M (Figure 3-2b). Thus, a sufficiently high HCl concentration was critical for triggering the sol-gel chemistry[32] of the PIPSMA homopolymer, and presumably also for the PIPSMA blocks of the block copolymers.

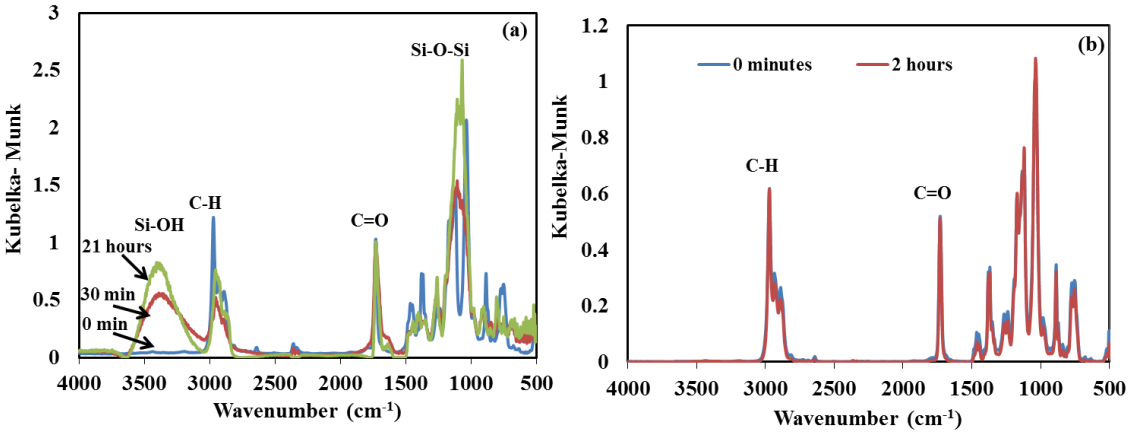

Figure 3-2 DRIFT-IR spectra of the PIPSMA homopolymer as it underwent sol-gel reactions at an HCl concentration of 6.2×10^{-1} M (a) and 1.0×10^{-3} M (b).

The effect of varying the HCl concentration on the formation of the diblock copolymer coatings was investigated by probing the morphology, surface composition, and amphiphobicity of the resultant coatings. Figure 3-3 compares representative AFM topography and phase images of an uncoated glass plate, and P1-2 coatings prepared at a fixed polymer amount of 1.95 μg/cm^2, but at different HCl concentrations in the final coating solution mixture consisting of TFT, P1-2 in TFT, and HCl in THF.

The phase images of the coatings prepared at HCl concentrations of 0.90×10^{-1} M and 0.90×10^{-2} M were homogeneous, suggesting the existence of only one component on the glass surface. In addition, their topography images were smooth with root-mean-square roughness R_{rms} values of 0.42 and 0.38 nm, respectively, which was comparable to the R_{rms} value of 0.28 nm observed for uncoated glass.[22] However, the surfaces became bumpier when the HCl concentration was decreased to 0.90×10^{-3} or 0.90×10^{-4} M, creating surfaces with R_{rms} values of 0.48 and 0.59 nm, respectively. This was probably due to the slower rate of the sol-gel chemistry exhibited by the PIPSMA block. The increase in surface bumps was accompanied by the appearance of contrast in the phase images, which suggests the presence of more than one species on the coating surface in these cases.

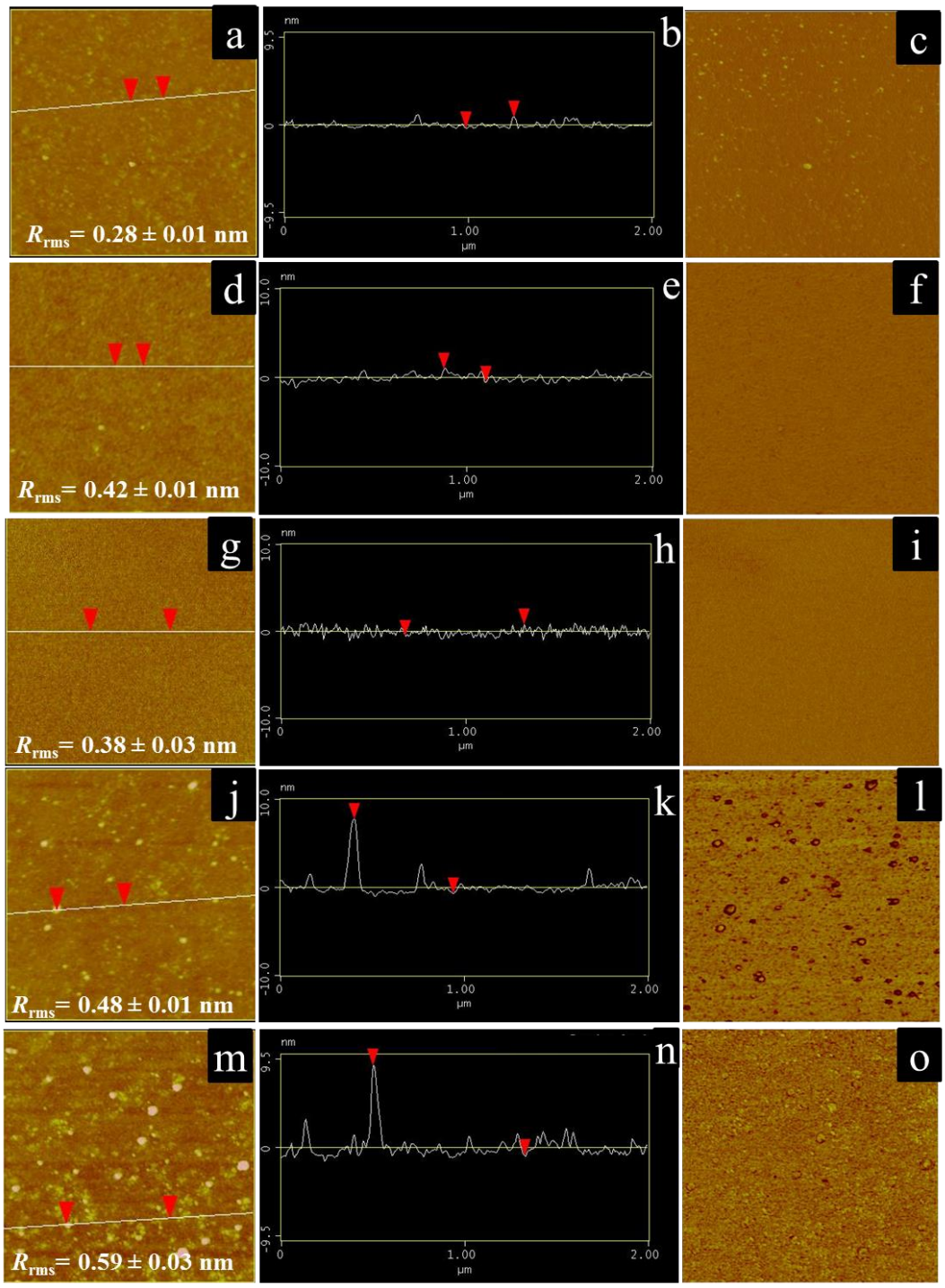

Figure 3-3 AFM height (a) cross-sectional (b) and phase (c) images of an uncoated clean glass plate and AFM height (d, g, j, and m), cross-sectional (e, h, k and n) and phase (f, i, l, and o) images of P1-2 coatings prepared at an amount of 1.95 µg/cm^2 but at different HCl concentrations: [HCl] = 0.90×10^{-1} (d, e, and f), 0.90×10^{-2} (g, h, and i), 0.90×10^{-3} (j, k, and l), and 0.90×10^{-4} M (m, n, and o). The height and phase angle delay ranges are 20 nm and 75^o, respectively, and the dimensions of the images are 2.0 × 2.0 µm^2.

The XPS data obtained for the P1-1 and P1-2 coatings prepared at HCl concentrations of 0.90×10^{-1} and 0.90×10^{-4} M and at copolymer amounts of 1.5 and 1.95 μg/cm^2 respectivly, are shown in Figure 3-4a. The survey XPS spectra clearly demonstrated that both of the coatings prepared at an HCl concentration of 0.90×10^{-4} M had a stronger intensity Si_{2p} peak than those prepared at an HCl concentration of 0.90×10^{-1} M. This difference suggested that the PIPSMA block had a higher probability to appear at the surface in the former cases. Furthermore, the area ratio between the F_{1s} and C_{1s} peaks increased when [HCl] increased from 0.90×10^{-4} to 0.90×10^{-1} M, indicating the higher surface PFOEMA amount in the coatings prepared in the latter case.

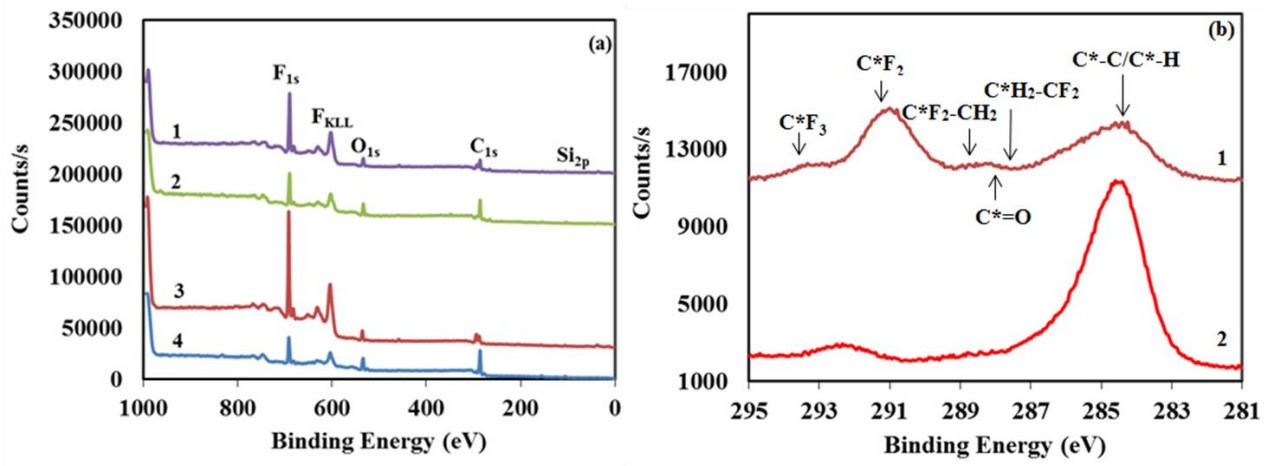

Figure 3-4 XPS survey spectra (a) of P1-1 and P1-2 coatings prepared at 1.50 and 1.95 μg/cm^2, respectively: P1-1 at [HCl] = 0.90×10^{-1} M (1), P1-1 at [HCl] = 0.90×10^{-4} M (2), P1-2 at [HCl] = 0.90×10^{-1} M (3), and P1-2 at [HCl] = 0.90×10^{-4} M (4). High-resolution C_{1s} spectra (b) of P1-2 coatings prepared at [HCl] of 0.90×10^{-1} M (1) and 0.90×10^{-4} M (2).

High-resolution C_{1s} spectra have also been obtained for the P1-2 coatings at HCl concentrations of 0.90×10^{-1} and 0.90×10^{-4} M (Figure 3-4b). Other elemental high resolution spectra can be seen in the Appendix. At HCl concentrations of 0.90×10^{-1} M, the areas of the CF_2 (291.5 eV) and CF_3 (293.6 eV) signals probed by XPS evidently increased relative to those of the carbonyl carbon (287.8 eV) or the carbon atoms that were bound with hydrogen (284.6 eV).[22,33-34] The integration of the different peaks

were determined and corrected by calibrating each peak in reference to the C_{1s} line located at 285.0 eV. Comparing the corrected areas yielded the atomic compositions of the two P1-2 coatings (Table 3-2). Increasing the HCl concentration from 0.90×10^{-4} to 0.90×10^{-1} M caused the F atomic composition to increase from 18.9% to 54.0%. Meanwhile, the C, O, and Si atomic compositions decreased from 59.5%, 15.7%, and 5.9% to 32.1%, 11.3%, and 2.6%, respectively.

Table 3-2 Surface atomic compositions probed by XPS for various coatings. The error in each case was ± 0.01%.

Sample	[HCl] (M)	Polymer Amount ($\mu g/cm^2$)	Atomic Concentration (%)			
			C	F	O	Si
P1-1	0.90×10^{-1}	1.50	51.4	36.9	9.1	2.5
P1-1	0.90×10^{-4}	1.50	61.4	21.2	13.4	4.0
P1-2	0.90×10^{-1}	1.95	32.1	54.0	11.3	2.6
P1-2	0.90×10^{-4}	1.95	59.5	18.9	15.7	5.9
P2	0.90×10^{-1}	1.50	34.2	45.0	15.7	5.1
PFOEMA	-	1.50	45.0	48.4	6.6	-

If PFOEMA was exposed at the surface of the coating and XPS only probed this layer, the following atomic compositions would have been detected: C = 42.4%, F = 51.5%, and O = 6.1%. These values were calculated based on the FOEMA molecular formula of $C_{14}F_{17}O_2$, where H atoms were excluded because they were not detected by XPS (high resolution spectra and AFM images are shown in the Appendix). While the calculated values were reasonably consistent with the observed values of C = 45.0%, F = 48.4%, and O = 6.6% for a PFOEMA film covering a glass plate (Table 3-2), they were different from those determined for a P1-2 coating prepared at an HCl concentration of 0.90×10^{-1} M. The high fluorine abundance of 54.0% for this coating suggested that the surface was mainly composed of the PFOEMA block. The F content was even higher than 51.5% calculated for PFOEMA, probably because the perfluorooctyl ethyl groups stretched outwardly from the coating into the air. Previous studies have concluded that the perfluorooctyl ethyl groups formed a liquid crystalline layer extending from PFOEMA surfaces.[35]

If sol-gel reactions had reached completion, each sol-gelled IPSMA unit would have had an effective formula of $C_7H_{11}SiO_{3.5}$. In this case, if the sol-gelled layer was probed via XPS as well, it would be anticipated that the diblock copolymer layer would have an atomic composition of F = 44.5%, C = 44.6%, O = 9.4%, and Si = 1.4%. Thus, the determined O and Si contents of 11.3% and 2.6%, respecitvely, in the coating prepared at an HCl concentration of 0.90×10^{-1} M were higher than the theoretical values anticipated for a pure PIPSMA layer. Three factors could have caused these differences. First, the underlying glass may have also been probed by XPS. Second, the coating did not have a perfect structure consisting of an exposed PFOEMA surface layer and a sol-gelled PIPSMA sub-layer. Instead, some of the sol-gelled PIPSMA units may have appeared on the coating surface. Third, a combination of both the first and second factors may have played a role. In the first scenario, the probing of the glass by XPS could be due to either the insufficient thickness of the brush layer, or the imperfect coverage of the substrate by the brush layer.

Unlike the coating prepared at an HCl concentration of 0.90×10^{-1} M, the coating prepared at an HCl concentration of 0.90×10^{-4} M had a substantially lower F content of 18.9%. This would be possible only if a large fraction of the PIPSMA chains existed on the coating surface, or if the glass substrate was not fully covered by the polymer. According to the FT-IR analysis, the PIPSMA homopolymer did not undergo sol-gel reactions at this HCl concentration. Thus, the PIPSMA block of P1-2 did not graft onto the glass plate, and could have been present in the surface layer. The AFM images of the coatings prepared at an HCl concentration of 0.90×10^{-4} M seemed to suggest that the glass was not fully covered, and also that some of the copolymer existed on the glass plates as nanoclusters.

We measured the static, advancing (θ_{adv}), and receding (θ_{rec}) CAs of water, diiodomethane, and hexadecane droplets on P1-2 coatings prepared at 1.95 μg/cm^2 and with different HCl concentrations. The SAs were also measured to determine the tilting angle above which a 20 μL droplet slid off a coated and tilted glass plate. The data obtained from these measurements are plotted in Figure 3-5. Also plotted are the ($\cos\theta_{rec} - \cos\theta_{adv}$) values for coatings prepared at different HCl concentrations. The ($\cos\theta_{rec} -$

$\cos\theta_{adv}$) values were plotted as they dictate the readiness for a droplet to slide.[22] As the HCl concentration was decreased, the CAs, the CAH ($\theta_{adv} - \theta_{rec}$), the SAs, and the ($\cos\theta_{rec} - \cos\theta_{adv}$) values all increased. These trends suggested that the repellency of the coatings had diminished. Therefore, the static and dynamic wetting data suggested that the resultant coating surfaces possessed a decreasing fluorine content as the HCl concentration was decreased.

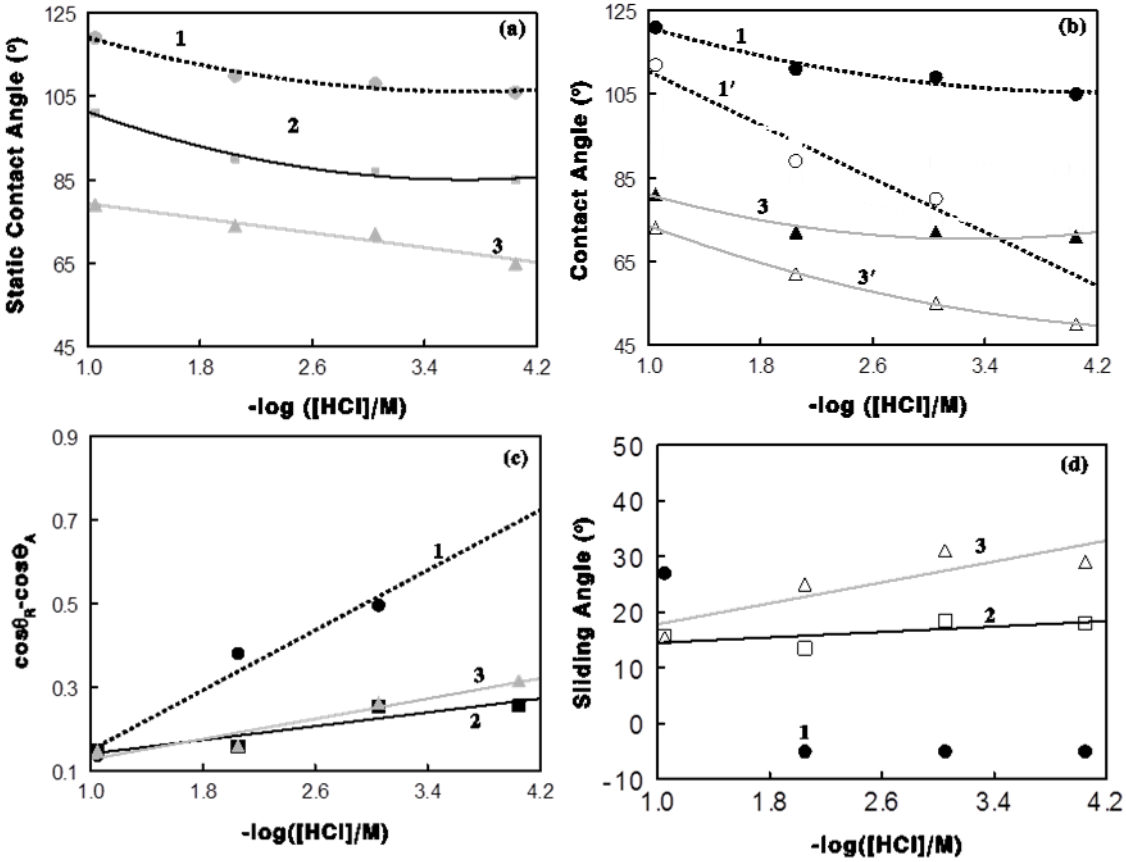

Figure 3-5 Effect of varying the HCl concentration on the static and dynamic wetting properties of P1-2 coatings prepared at a polymer amount of 1.95 μg/cm^2: SCA variation (a) for water (1), diiodomethane (2), and hexadecane (3). θ_{adv} and θ_{rec} angle variation (b) for water (1 and 1') and hexadecane (3 and 3'). ($\cos\theta_{rec}$ - $\cos\theta_{adv}$) variation (c) for water (1), diiodomethane (2), and hexadecane (3). SA variation (d) for 20-μL droplets of water (1), diiodomethane (2), and hexadecane (3). Negative SAs indicated that the water droplets did not slide off the glass plates.

We also obtained from XPS atomic compositions of P1-1 coatings prepared at 1.50 μg/cm^2 but at HCl concentrations of 0.90×10^{-1} and 0.90×10^{-4} M, respectively. The variation in the atomic

composition with the HCl concentration (Table 3-2) mirrored those observed for the P1-2 coatings. Thus, all of the coatings discussed below were prepared at an HCl concentration of 0.90×10^{-1} M.

3.5 Effect of Varying the Polymer Amount

It was imagined that insufficient use of P1-2 would yield "patches" or "islands" of the coating that only partially covered the glass. Increasing the amount of P1-2 would first produce a loosely-packed P1-2 layer and would eventually yield a crowded brush layer. In a crowded brush layer, the sol-gelled PIPSMA block would become grafted and crosslinked onto the glass, and the PFOEMA block would stretch outwardly into the solvent phase. Of course, the PFOEMA chains would eventually collapse after solvent evaporation. Increasing the P1-2 amount beyond the limit required for a saturated brush would also produce some nanoclusters on the surface of the brush. These clusters should consist of a sol-gelled PIPSMA core that is surrounded by a PFOEMA corona. Since they were physically deposited onto the brush layer and not covalently attached, they could be easily removed and would not contribute to the long-term amphiphobicity of the surface. Therefore, the goal was to provide sufficient copolymer to ensure that a saturated monolayer had formed, while avoiding the use of excess amounts of the copolymer and the formation of nanoclusters. Careful control of the amount of copolymer employed could thus enhance the efficiency of the coating process and avoid waste of the expensive fluorinated block copolymer.

To estimate the amount of P1-2 required to form a saturated brush layer, we assumed a fully stretched length of 11.8 nm for a chain consisting of 13 PIPSMA units and 30 PFOEMA units.[19,36-37] Using the average density of 1.85 g/cm^3 for the PFOEMA and sol-gelled PIPSMA blocks (Appendix),[38] we estimated that 2.81 μg of P1-2 was required to prepare a sol-gelled P1-2 film that was 11.8 nm thick and covered an area of 1.3 cm^2. In reality, the polymer forming a brush layer would not be as dense as a

polymer encountered in the solid state.[39] Thus, we used P1-2 amounts typically less than this value to achieve a brush coating.

Figure 3-6 compares AFM topography and phase images of P1-2 coatings prepared at the polymer amounts of 0.76, 1.15, 1.62, and 2.31 μg/cm^2, respectively. Examining these images and those shown in Figure 3-2 prepared at 1.95 μg/cm^2 suggests the following trend. At a low polymer amount of 0.76 μg/cm^2, the coating was rough as revealed by the tomography image shown in Figure 3-6a. The phase image shown in Figure 3-6b suggested that the coating was chemically heterogeneous. As greater amounts of polymer were used, the surface composition heterogeniety (as revealed by the phase images) decreased. The surface roughness initially decreased with the amount of polymer. As the polymer amount reached 2.31 μg/cm^2, the surface became rough again despite the homogeneous surface composition as revealed by the phase image. This observation indicated that the excess polymer chains would simply form multiple layers while the coating properties remained unchanged. Hence, less polymer was needed to form a thin brush layer than expected.

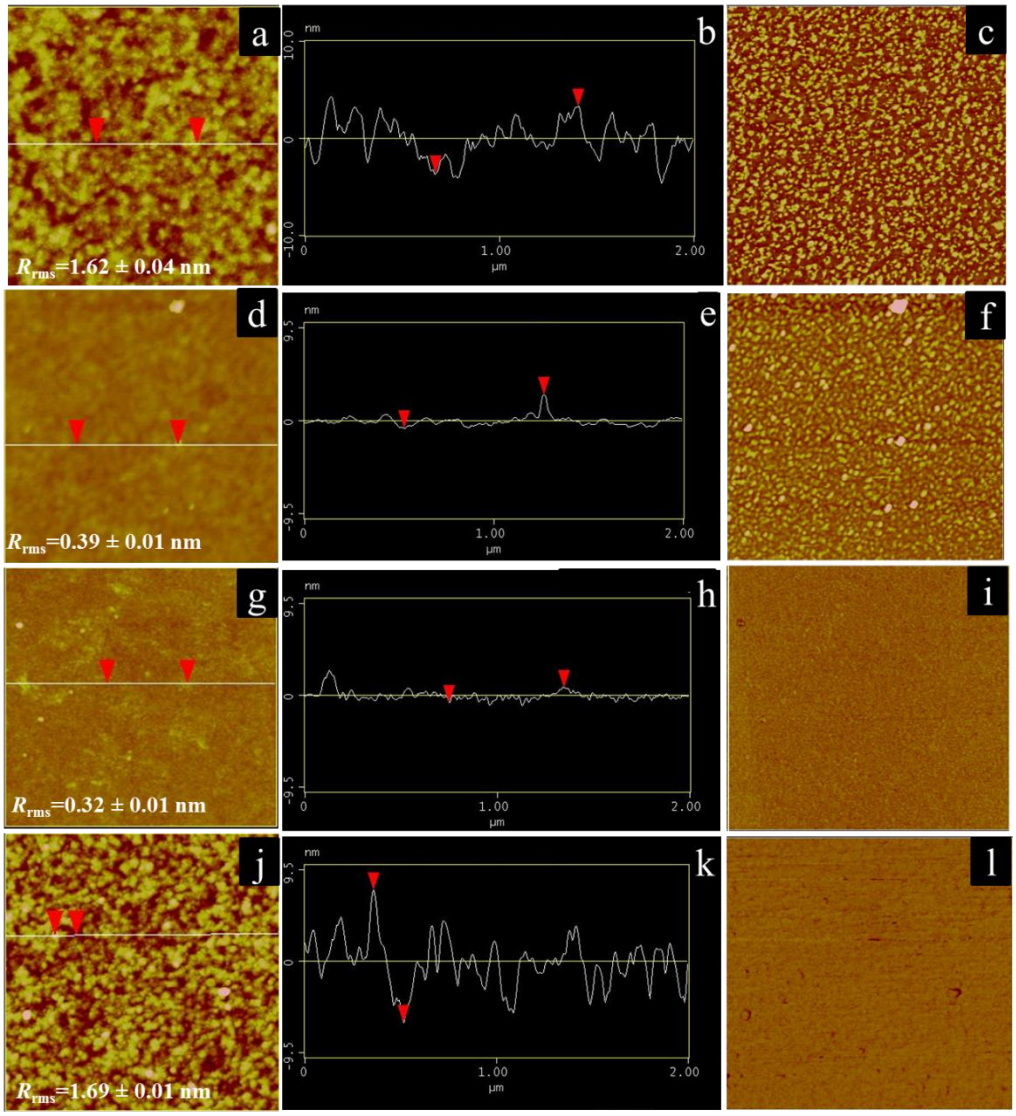

Figure 3-6 AFM topography (a, d, g, and j), cross-sectional (b, e, h, and k) and phase (c, f, i, and l) images of P1-2 coatings prepared at an HCl concentration of 0.90×10^{-1} M but at different polymer amounts. The used polymer amounts were 0.76 (a, b, and c), 1.15 (d, e, and f), 1.62 (g, h, and i), and 2.31 μg/cm^2 (j, k, and l). The height and phase angle delay ranges are 20 nm and 75^o, respectively, and the dimensions of the image are 2.0 × 2.0 μm^2.

The trends observed with the AFM images supported our proposed effect of varying the polymer amount on the structure of the resultant coating. The surface was rough at low P1-2 amounts because only a patchy sub-monolayer was formed. Since only certain regions of the glass plate were covered by P1-2, two types of surface compositions (glass vs. polymer) were probed via AFM in the phase mode. Above a certain polymer amount in the coating formulation, the glass was fully covered by P1-2. Thus,

the surface roughness and phase contrast decreased. Increasing the P1-2 amount beyond what was needed for a saturated monolayer produced not only a brush layer, but also yielded some nanoclusters. Thus, the surface roughness increased again. Since both the nanoclusters and the brush layer had a PFOEMA surface, the surface composition as probed via AFM in the phase mode remained homogeneous.

The surface compositional homogeneity above a certain P1-2 amount was supported by the static and dynamic wetting properties determined for the coated glass samples (Figure 3-7). The static, θ_{adv}, and θ_{rec} angles of the three testing liquids (water, diiodomethane, and hexadecane) all increased initially with the P1-2 amount. Above 1.60 μg/cm^2, these angles plateaued. In addition, the CAH and the ($\cos\theta_{rec} - \cos\theta_{adv}$) values initially decreased and then plateaued above 1.60 μg/cm^2. This plateauing trend was resonated by the SA data for water as well.

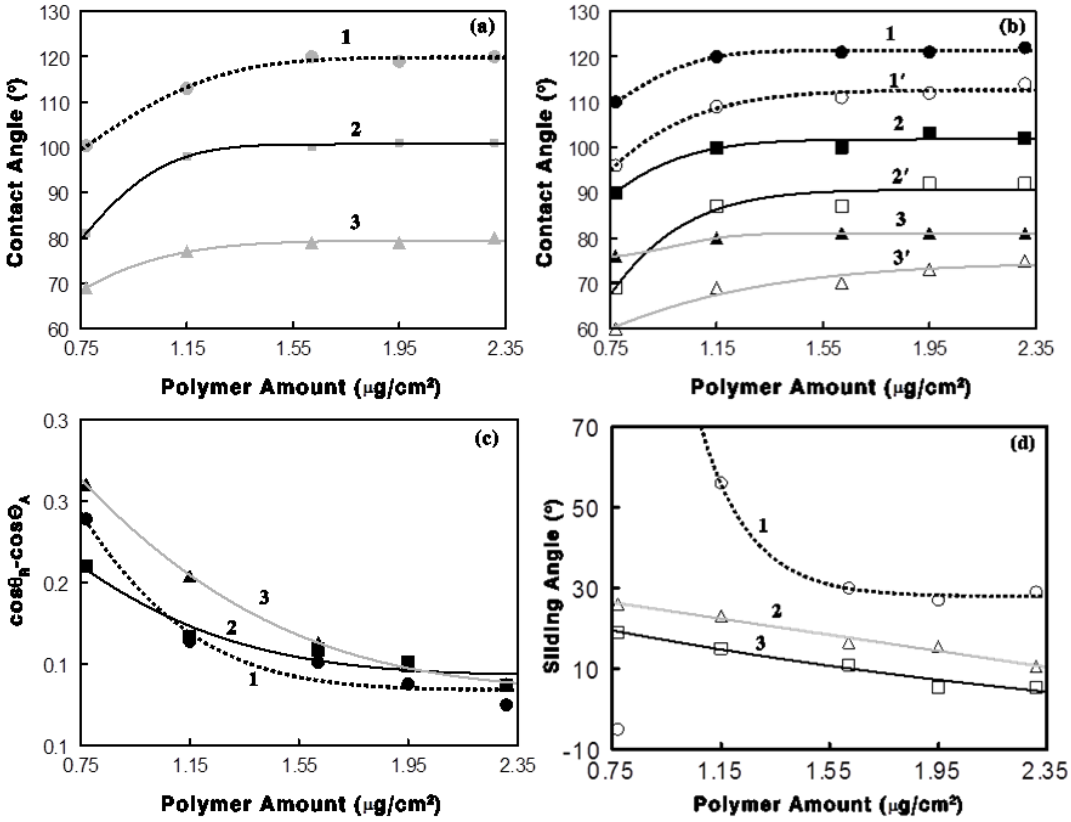

Figure 3-7 Effect of varying the polymer amount on the static and dynamic wetting properties of P1-2 coatings prepared at an HCl concentration of 0.90×10^{-1} M: SCA variation (a) for water (1), diiodomethane (2), and hexadecane (3). θ_{adv} and θ_{rec} angle variation (b) for water (1 and 1'), diiodomethane (2 and 2'), and hexadecane (3 and 3'). ($\cos\theta_{rec}$ - $\cos\theta_{adv}$) variation (c) for water (1), diiodomethane (2), and hexadecane (3). SA variation (d) for 20-μL droplets of water (1), diiodomethane (2), and hexadecane (3). The negative SA in (d) suggests that the water droplets did not slide off the glass plates.

In summary, a saturated brush layer seemed to form from P1-2 at 1.65 μg/cm^2. To ensure the formation of a saturated brush layer, a P1-2 amount of 1.95 μg/cm^2 was used to obtain the results reported in the rest of this thesis.

3.6 Effect of Varying the Fluorinated Agents

P1-1 and P2 were also used to fluorinate the glass plates. To ensure a saturated brush layer had formed in each case, the polymer amount of 1.50 μg/cm^2 was used for P1-1 and P2, respectively. This

amount was less than 1.95 μg/cm^2 used for P1-2. This value differed because P1-2 chains were the longest among the copolymers, and thus P1-2 had the highest molecular weight among the three reagents. Therefore, it was anticipated that P1-2 should form a saturated brush coating. We confirmed that 1.50 μg/cm^2 was sufficient for a saturated P1-1 brush by comparing water SCAs on coatings prepared at 1.50 and 2.00 μg/cm^2, respectively. The water CA values were similar at 115 ± 1˚ on the two types of coatings.

Glass plates coated by P1-1, P1-2, and P2 were all optically clear. Between 500-550 nm, the transmittances of the coated glass plates were all higher than 89.6%, which was measured for an uncoated glass plate.[25,40] For glass plates coated by P1-1, P1-2, and P2, the transmittances were 90.2%, 91.3% and 91.6%, respectively (Figure 3-8a). The optical clarity was further confirmed by the fact that writing placed underneath the coated glass plates was clearly visible (Figure 3-8b). The transmittance increased for the coated glass plates because the fluorinated polymers had refractive indices between those of glass (1.51) and air (1.00).[41] This graduated decrease in the refractive index from the glass to air helped suppress light loss due to interfacial reflectance.[22,25]

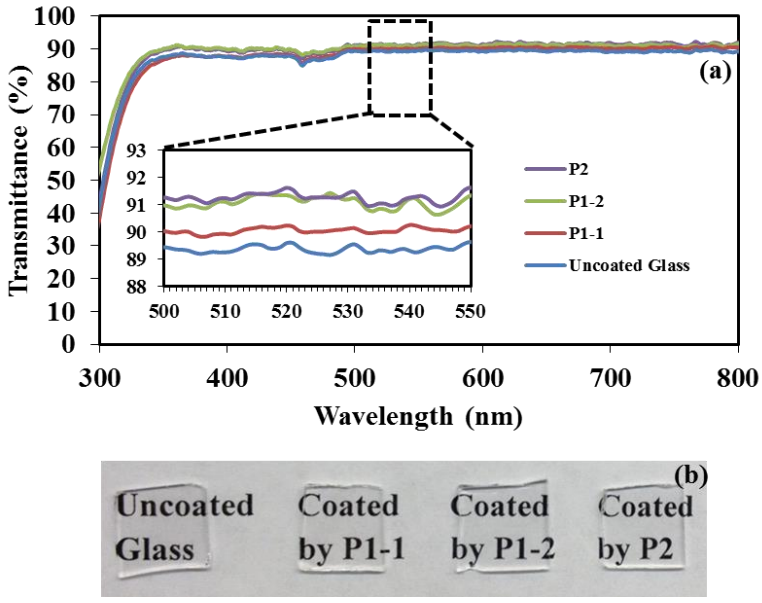

Figure 3-8 UV-Vis transmittance spectra (a) of a clean uncoated glass plate and of glass plates that were coated with P1-1, P1-2, and P2. The inset shows a magnification of the spectra in the wavelength range of 500-550 nm. Also shown is a photograph (b) of an uncoated glass plate and glass plates that were coated with different copolymers under optimized conditions.

AFM analysis was performed on the glass plates coated by P1-1 and P2 as seen in Figure 3-9, which displays both height and phase images. Both coatings were rather smooth with low R_{rms} values. This indicated that the HCl concentration of 0.90×10^{-1} M was also appropriate for other diblock copolymer systems with varying molecular weights.

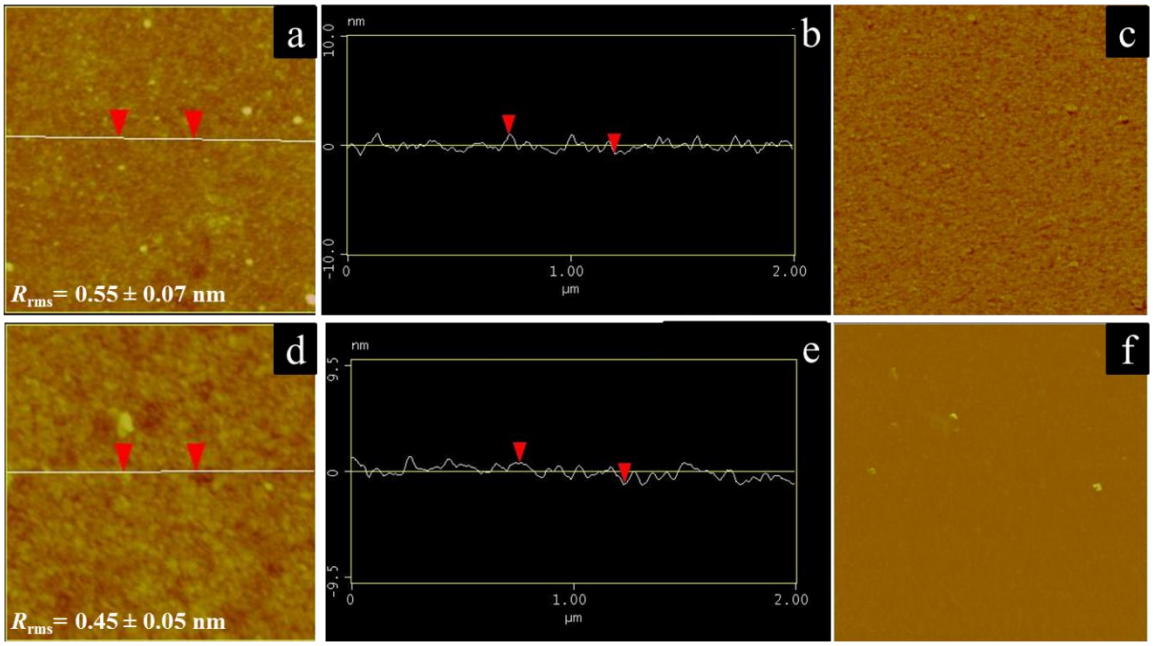

Figure 3-9 AFM 2.0×2.0 μm^2 topography (a and d), cross-sectional (b and e), and phase (c and f) images of glass plates coated with P1-1 (a, b, and c) and P2 (d, e, and f) at an HCl concentration of 0.90×10^{-1} M. The height and phase delay ranges for the images are 20 nm and 75^o, respectively.

The P1-1 and P2 coatings were also analyzed by XPS (high resolution spectra are shown in Appendix). According to Table 3-2, the P1-1 coating had C and F atomic compositions of 51.4% and F = 36.9%, respectively. Consequently, this coating had a higher C content but a lower F content than that of the P1-2 coating, in which the respective values were 32.1% and 54.0%. We suspect that this difference was caused by the reduced ability of the thin PFOEMA layer in a P1-1 brush to block the XPS electrons from reaching the underlying sol-gelled PIPSMA block and the glass.

XPS analysis of the P2 coating indicated that it had C, F, O, and Si atomic compositions of 34.2%, 45.0%, 15.7%, and 5.1%, respectively. The fluorinated PFPO domain of P2 (Scheme 1) has the formula $C_{44}F_{89}O_{14}$ (excluding H) and thus the theoretical compositions of C = 29.9%, F = 60.5%, and O = 9.5%. Evidently, the measured F content was much lower than that calculated for PFPO, suggesting that XPS was able to probe species existing beneath the PFPO layer. If PIPSMA had undergone complete sol-gel reactions and was fully probed by XPS, the effective formula for grafted P2 excluding H should be $C_{90}F_{89}Si_6O_{37}Br$. If this was the case, the atomic composition should be C = 40.4%, F = 39.9%, Si = 2.7%, and O = 16.6%. The fact that the determined F content of 45.0% was closer to the F content of 39.9%, suggests that the PFPO layer was thin, and the sol-gelled PIPSMA layer was indeed probed by XPS.

Conclusions reached from the XPS data were supported by the wettabilities of these coatings. Figure 3-10 compares the static, θ_{adv}, and θ_{rec} CAs as well as the ($\cos\theta_{rec}$ - $\cos\theta_{adv}$) and SA data for water, diiodomethane, and hexadecane on glass plates coated by different polymers. The P1-2 coatings clearly possessed the highest CAs, and the lowest SAs. On the other hand, the P2 coatings had the lowest SCAs and the highest CAH for water droplets. Despite their low SCAs, the P2 coatings had low ($\cos\theta_{rec}$ - $\cos\theta_{adv}$) and SA values when tested against both diiodomethane and hexadecane.

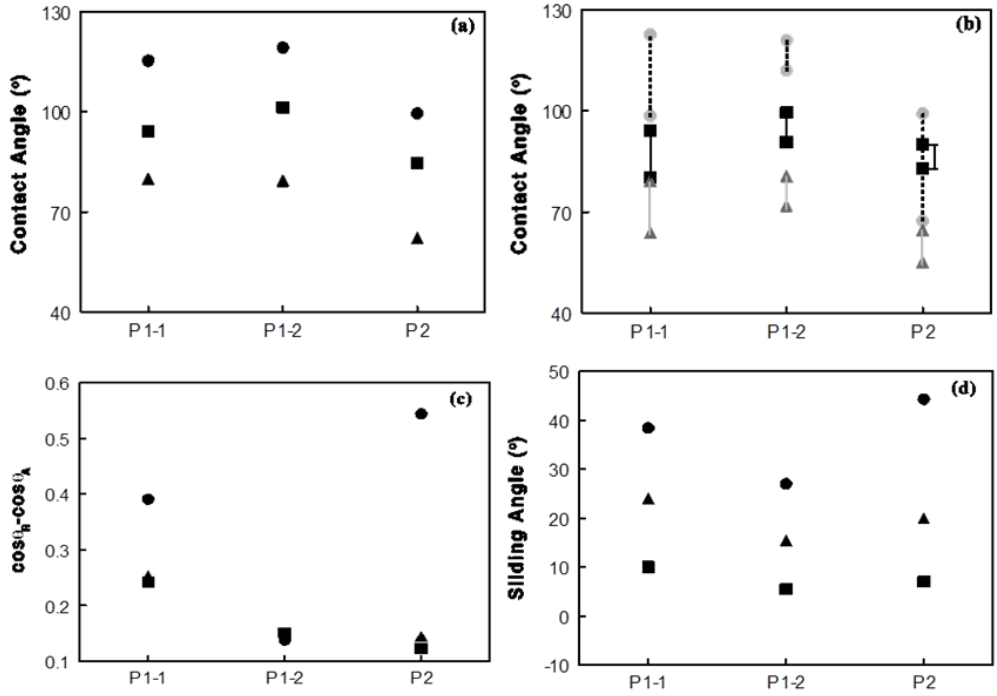

Figure 3-10 Comparison of the static and dynamic wetting properties of coatings prepared from P1-1, P1-2, and P2 at an HCl concentration of 0.90×10^{-1} M. SCA variation (a) for water (•), diiodomethane (■), and hexadecane (▲). θ_{adv} and θ_{rec} angle variation (b) for water (•), diiodomethane (■), and hexadecane (▲). Variation in ($\cos\theta_{rec}$ - $\cos\theta_{adv}$) values (c) for water (•), diiodomethane (■), and hexadecane (▲). SA variation (d) for 20 μL droplets of water (•), diiodomethane (■), and hexadecane (▲).

P1-2 was more amphiphobic than P1-1 because P1-2 had a longer PFOEMA block than the latter copolymer. Meanwhile, P2 had lower SCAs than the P1 family of polymers because its PFPO fluorinated block differed from the PFOEMA blocks of the P1 polymers. PFPO has a higher surface tension than PFOEMA, and thus it would be anticipated that liquids would exhibit lower CAs on PFPO.[42] Despite their lower SCAs, the ($\cos\theta_{rec}$ - $\cos\theta_{adv}$) values were low on the P2 coatings for diiodomethane and hexadecane because PFPO is "liquid-like". The constant motion of the PFPO chains caused the surfaces of the P2 coatings to appear dynamically homogeneous when probed over the time scale of liquid movement.[22] The large ($\cos\theta_{rec}$ - $\cos\theta_{adv}$) value observed for water droplets was surprising considering that they were measured on perfluorinated polyether surfaces.[43] This was probably due to the thinness of the PFPO layer. The movement of the PFPO chains may have exposed the underlying sol-gelled hydrophilic PIPSMA layer, which pinned the water droplets and led to hysteresis.

3.7 Dynamic Non-Wetting and Anti-Smudge Properties

The amphiphobicity of the brush coatings could be appreciated by comparing the photographs taken of water and hexadecane droplets at different times after the liquid had been dispensed onto a P1-2 coated plate at the slanting angles of 30˚ and 19˚, respectively (Figure 3-11). No liquid residue remained behind after the droplet glided down the coated glass plate. Thus, this surface manifests its repellency not in a high droplet CA, but through the efficient sliding down of a droplet as a whole. In contrast to this efficient sliding behaviour, a hexadecane droplet spread outwardly on an uncoated slanted glass plate leaving behind oil streaks that marked its pathway.

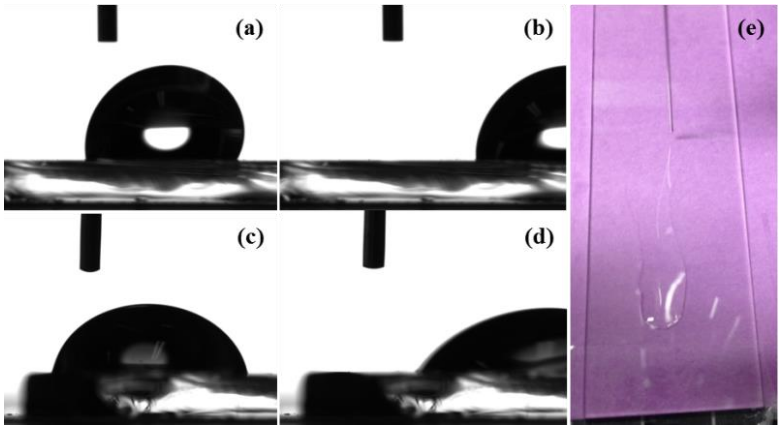

Figure 3-11 Photographs of water (a and b) and hexadecane (c and d) droplets after they had been dispensed onto P1-2 coated glass plates. The time lag between (a) and (b), and (c) and (d), were 17 and 9 s, respectively. The dark cylindrical object at the upper left corner of each photograph was the stationary syringe needle tip. The glass plate slanting angles were 30˚ and 19˚, respectively. Image (e) shows that hexadecane spread over, rather than slid along an uncoated glass plate.

All of the tested coatings did not have high water or oil CAs because they were flat and lacked high surface areas and re-entrant surface features.[44] However, they exhibited excellent dynamic non-wetting properties as characterized by the low SAs, low CAH, and low ($\cos\theta_{rec}$ - $\cos\theta_{adv}$) values when they were tested against liquid droplets. Superior dynamic wetting properties are normally associated with homogeneous surfaces.[22] The coatings were topographically homogeneous because they were flat. The P1-1 and in particular the P1-2 coatings, were chemically homogeneous because their surfaces were

dominated by the PFOEMA chains. In the case of the P2 coatings, although the PFPO chains were insufficiently long to fully cover the sol-gelled PIPSMA block, the coatings should still be chemically homogeneous because of the dynamic nature of the PFPO chains.[45] The fast segmental rotation of the PFPO chains would even out potential compositional differences at different locations and yield a constant time-average composition for each site on the surface. This explained their superior dynamic non-wetting properties towards hexadecane and diiodomethane just as has been reported by other researchers for surfaces modified by poly(*n*-hexafluoropropyloxide) or demnum chains.[46-47] The large CAH and SA values observed for water droplets on P2 coatings here could be due to strong attraction between the sol-gelled PIPSMA layer and the inability of the short PFPO chains to fully shield the PIPSMA layer or the glass plate.

This superior oil repellency of the P2 coatings was further demonstrated by an anti-writing test, which involved writing on glass plates using a Sharpie® permanent oil-based black marker. On an uncoated glass plate, the written lines were evidently thicker than those left on plates coated by P1-1 and P1-2 (Figure 3-12). Intriguingly, the written lines that had been applied onto P2-coated glass plates shrank within fractions of a second and the final stabilized written lines were much fainter than those left on plates that had been coated by P1-1 or P1-2.

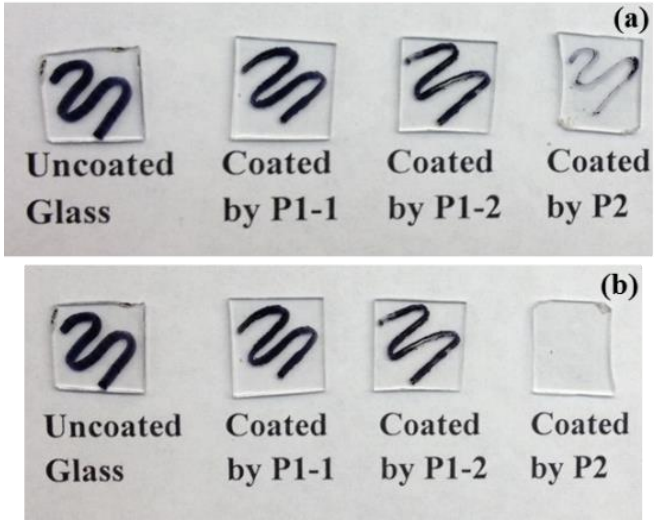

Figure 3-12 Photographs of uncoated glass plates and those coated using different polymers after they had been written on with a black permanent marker (a) and subsequently rubbed with a tissue (b).

After the lines of ink dried, a fresh piece of tissue paper was used to clean the writings. Evidently, the writing could not be removed from the uncoated glass plate, and thus they were effectively "permanent" markings. These markings were not removed from the plates coated by P1-1 and P1-2 either. In stark contrast, the markings were more readily removed from plates coated by P2.

The P2-coated plates were not only more resistant to writing, but also the resultant markings were more readily removed from P2-coated plates. We imagined that ink that was written on a P2-coated glass plate would easily shrink because the PFPO layer is a fluorinated liquid.[45] The shrinking motion of the ink droplet was facilitated not only by the liquid droplet itself, but also by the chains that constituted the substrate. The ink was more readily removed again because of the mobile nature of the PFPO chains, which helped push the ink patches upwardly from "crevices" that were normally found in a solid substrate. Thus, the dynamic nature of a liquid substrate facilitates the release of the ink and presumably other dirt or smudge.

The process of writing and rubbing away the ink was repeated ten times on a P2-coated glass plate. The SCA was then measured using water and diiodomethane droplets. There was almost no change in the CAs. The fact that the process of writing and ink removal could be repeated ten times and that no changes in the CAs for water and diiodomethane were observed, suggested that the P2 coatings were robust.

3.8 Durability of the Coatings

In order to evaluate whether the sol-gel chemistry of the PIPSMA block was effective, the coated plates were stirred overnight in a TFT solution to remove any excess or unused polymer, and to determine whether the PIPSMA block was in fact covalently grafted onto the surface (Appendix). The wetting properties of the P1-2-coated plates did not change throughout this process. Before TFT extraction, the plates exhibited a water SCA of 119.0˚ ± 1˚, and after extraction, the plates exhibited a water SCA of

118.7˚ ± 1˚. The fact that the amphiphobic properties were retained indicated that the PIPSMA block had indeed become grafted onto the glass substrate.

The durability of the coated glass plates was tested using a homemade mechanical device as shown in Chapter 2. This device had cotton fabric mounted on a rotating probe to rub the films with 500 g of force. After the films had been tested for allotted times of 1 min (40 rotations), 5 min (200 rotations) and 1 h (2400 rotations) with the device, it was apparent that the P2-based films were the most robust. In particular, the water CAs of the P2-based films remained unchanged after the rubbing tests, and the ink applied onto these coatings during the anti-writing test still shrank readily. This was likely due to the "liquid-like" state of the PFPO block. The PFPO block was able to withstand abrasion because of the low friction coefficient of approximately 0.1 that it possesses.[48] This lower coefficient of friction is due to the lower resistance offered to the shearing action and the lubrication properties of PFPE molecules themselves.[49] The results are summarized in Table 3-3.

Table 3-3 Durability test results showing the change in water CA before and after the coated films were subjected to rubbing tests for after 1 min, 5 min, and 1 h. The error in each case was ± 2˚.

Sample	Before Rubbing (˚)	After 1 minute (˚) 40 rotations	After 5 minutes (˚) 200 rotations	After 1 hour (˚) 2400 rotations
P1-1	115	95	55	50
P1-2	118	108	90	90
P2	100	100	100	100

In contrast, the hydrophobicity of the P1-1 and P1-2 films seemed to degrade even after they had been subjected to rubbing tests for only a short span of time. A decrease in the water CA suggested that some, but not all, of the coating had been removed as the plates still demonstrated hydrophobic properties. After 5 min to 1 h, the P1-2 films still remained hydrophobic whereas the P1-1 films did not. This diminished performance was probably due to the decrease in the fluorinated units. Since a monolayer

was being formed, these films were quite thin. Therefore, these films may not have been able to withstand abrasion for long periods of time.

References

1. De Gennes, P.-G.; Brochard-Wyart, F.; Quéré, D. *Capillarity and Wetting Phenomena: Drops, Bubbles, Pearls, Waves*. Springer: New York, **2004**.
2. Jin, C.; Jiang, Y.; Niu, T.; Huang, J. *J. Mater. Chem.* **2012,** *22*, 12562-12567.
3. Andreas, S.; Zdenek, C.; Boris, F. S.; Manuel, S.; Wilhelm, B. *Bioinspir. Biomim.* **2007,** *2*, S126.
4. Wang, C.; Yao, T.; Wu, J.; Ma, C.; Fan, Z.; Wang, Z.; Cheng, Y.; Lin, Q.; Yang, B. *ACS Appl. Mater. Interfaces* **2009,** *1*, 2613-2617.
5. Celia, E.; Darmanin, T.; Taffin de Givenchy, E.; Amigoni, S.; Guittard, F. *J. Colloid Interface Sci.* **2013,** *402*, 1-18.
6. Kota, A. K.; Choi, W.; Tuteja, A. *MRS Bull.* **2013,** *38*, 383-390.
7. Nagappan, S.; Park, S. S.; Yu, E. J.; Cho, H. J.; Park, J. J.; Lee, W.-K.; Ha, C.-S. *J. Mater. Chem. A* **2013,** *1*, 12144-12153.
8. Zhang, Z.; Zhu, X.; Yang, J.; Xu, X.; Men, X.; Zhou, X. *Appl. Phys. A* **2012,** *108*, 601-606.
9. Butt, H.-J.; Semprebon, C.; Papadopoulos, P.; Vollmer, D.; Brinkmann, M.; Ciccotti, M. *Soft Matter* **2013,** *9*, 418-428.
10. Valipour Motlagh, N.; Birjandi, F. C.; Sargolzaei, J.; Shahtahmassebi, N. *Appl. Surf. Sci.* **2013,** *283*, 636-647.
11. Geng, Z.; He, J.; Xu, L.; Yao, L. *J. Mater. Chem. A* **2013,** *1*, 8721-8724.
12. He, Z.; Ma, M.; Lan, X.; Chen, F.; Wang, K.; Deng, H.; Zhang, Q.; Fu, Q. *Soft Matter* **2011,** *7*, 6435-6443.
13. Muthiah, P.; Bhushan, B.; Yun, K.; Kondo, H. *J. Colloid Interface Sci.* **2013,** *409*, 227-236.
14. Hikita, M.; Tanaka, K.; Nakamura, T.; Kajiyama, T.; Takahara, A. *Langmuir* **2005,** *21*, 7299-7302.
15. Kondo, H.; Sungkil, L.; Hanaoka, H. *Tribol. Trans.* **2008,** *52*, 29-35.
16. Xiong, D.; Liu, G.; Scott Duncan, E. J. *Polymer* **2013,** *54*, 3008-3016.
17. Hougham, G. *Fluoropolymers 2*. Springer: New York **2002**.
18. Nishino, T.; Meguro, M.; Nakamae, K.; Matsushita, M.; Ueda, Y. *Langmuir* **1999,** *15*, 4321-4323.
19. Hirao, A.; Sugiyama, K.; Yokoyama, H. *Prog. Polym. Sci.* **2007,** *32*, 1393-1438.
20. Renner, R. *Environ. Sci. Technol.* **2006,** *40*, 12-13.
21. Seed, B. Silanizing Glassware. In *Current Protocols in Cell Biology*, John Wiley & Sons, Inc.: 2001.
22. Cheng, D. F.; Masheder, B.; Urata, C.; Hozumi, A. *Langmuir* **2013,** *29*, 11322-11329.
23. Bhushan, B.; Muthiah, P. *Microsyst. Technol.* **2013,** *19*, 1261-1263.
24. Bravo, J.; Zhai, L.; Wu, Z.; Cohen, R. E.; Rubner, M. F. *Langmuir* **2007,** *23*, 7293-7298.
25. Urata, C.; Masheder, B.; Cheng, D. F.; Hozumi, A. *Langmuir* **2013,** *29*, 12472-12482.
26. Fabbri, P.; Messori, M.; Montecchi, M.; Pilati, F.; Taurino, R.; Tonelli, C.; Toselli, M. *J. Appl. Polym. Sci.* **2006,** *102*, 1483-1488.
27. Krishnan, S.; Kwark, Y.-J.; Ober, C. K. *Chem. Rec.* **2004,** *4*, 315-330.
28. Osterholtz, F. D.; Pohl, E. R. *J. Adhesion Sci. Technol.* **1992,** *6*, 127-149.
29. Savard, S.; Blanchard, L. P.; Leonard, J.; Prudhomme, R. E. *Polym. Compos.* **1984,** *5*, 242-249.
30. Haynes, W. M. *CRC Handbook of Chemistry and Physics* 94th ed.; CRC Press: Taylor and Francis Group: Boca Raton, Florida, **2013**.
31. Robert, M. S.; Francis, X. W.; David, J. *Spectrometric Identification of Organic Compounds*. 7th ed.; John Wiley and Sons: United States, **2005**.
32. Hench, L. L.; West, J. K. *Chem. Rev.* **1990,** *90*, 33-72.
33. Moulder, J. F.; Stickle, W. F.; Sobol, P. E.; Bomben, K. D. *Handbook of X-Ray Photoelectron Spectroscopy: A Reference Book of Standard Spectra for Identification and Interpretation of XPS Data*. Perkin-Elmer: Boca Raton, FL: **1992**.

34. Crist, B. V. *Handbook of Monochromatic XPS Spectra, The Elements of Native Oxides*. XPS International: CA, United States, **1999**.
35. Gao, Y.; Li, X.; Hong, L.; Liu, G. *Macromolecules* **2012,** *45*, 1321-1330.
36. Zhang, D.; Ortiz, C. *Macromolecules* **2004,** *37*, 4271-4282.
37. Xiong, D.; Liu, G.; Duncan, E. J. S. *ACS Appl. Mater. Interfaces* **2012,** *4*, 2445-2454.
38. Kim, J.; Efimenko, K.; Genzer, J.; Carbonell, R. G. *Macromolecules* **2007,** *40*, 588-597.
39. Zhao, B.; Brittain, W. J. *Prog. Polym. Sci.* **2000,** *25*, 677-710.
40. Karlsson, T.; Roos, A.; Ribbing, C. G. *Sol. Energ. Mater.* **1985,** *11*, 469-478.
41. Menzel, G. Inc., T. F. S., Ed. Braunschweig, Germany, 2011.
42. Messori, M.; Toselli, M.; Pilati, F.; Fabbri, P.; Pasquali, L.; Montecchi, M.; Nannarone, S.; Tonelli, C. *Surf. Coat. Int. Pt B-C.* **2005,** *88*, 243-249.
43. Block, S.; Hupfield, P.; Itami, Y.; Kitaura, E.; Kleyer, D.; Masutani, T.; Nakai, Y. New Anti-Fingerprint Coatings. *PCI Mag.* 2008, pp 88-92.
44. Tuteja, A.; Choi, W.; McKinley, G. H.; Cohen, R. E.; Rubner, M. F. *MRS Bull.* **2008,** *33*, 752-758.
45. Sianesi, D.; Zamboni, V.; Fontanelli, R.; Binaghi, M. *Wear* **1971,** *18*, 85-100.
46. Hamada, T. *Phys. Chem. Chem. Phys.* **2000,** *2*, 115-122.
47. Rudnick, L. R. *Synthetics, Mineral Oils, and Bio-Based Lubricants: Chemistry and Technology, Second Edition.* Taylor & Francis: Boca Raton, FL, **2013**.
48. Satyanarayana, N.; Gosvami, N. N.; Sinha, S. K.; Srinivasan, M. P. *Philos. Mag.* **2007,** *87*, 3209-3227.
49. Satyanarayana, N.; Sujeet, K. S. *J. Phys. D* **2005,** *38*, 3512.

Chapter 4

Summary and Conclusions

4.1 Fabrication of Anti-Smudge Polymer Brush Coatings on Glass Surfaces

This thesis describes the preparation of smooth and optically clear amphiphobic coatings covering glass substrates using three diblock copolymers (P1-1, P1-2, and P2). These copolymers were previously synthesized and characterized and were of the structure GX_n-*b*-FL_m that incorporated a grafting/crosslinking block of *n* GX units that was covalently bound to a fluorinated block of *m* FL units. With the GX block anchored onto the glass substrate and the overlying low surface energy FL block exposed at the surface, the coatings were rendered amphiphobic and exhibited anti-smudge properties. To prepare the coatings, a dilute copolymer solution in TFT was mixed with an HCl solution in THF and was subsequently deposited onto a glass plate. The solvent slowly evaporated, thus yielding a diblock copolymer film. Under these acidic conditions, the reactive triisopropyl groups located on the PIPSMA block were cleaved via sol-gel reactions to produce Si-OH groups that could react with the glass substrate, or with other reactive groups on other PIPSMA chains. Upon further reactions, Si-O-Si bonds were formed to create a crosslinked network. At sufficiently high HCl concentrations (e.g., at 0.090 M), a stable layer that resisted overnight extraction by TFT was formed. This stability was due to sol-gel reactions involving the PIPSMA block that caused this block to form a grafted and crosslinked layer on the glass plate.

As the amount of copolymer per unit glass area increased in the system, the static, θ_{adv}, and θ_{rec} CAs of water, diiodomethane, and hexadecane droplets on the surface initially increased, while the CAH initially decreased. However, these values plateaued once the amount of copolymer exceeded that required for the formation of a diblock copolymer brush layer or a monolayer (~1.60 μg/cm^2 for P1-2 coatings). Under optimized coating conditions, the copolymers formed monolayers. It was shown by XPS characterization that these monolayers bore fluorinated blocks as the exposed surface layers. In addition,

AFM characterization demonstrated that these monolayers were smooth, while spectroscopic analysis indicated that these coatings were optically clear in the visible light region. On account of its long PFOEMA block, P1-2 coatings exhibited higher SCAs and lower CAH values or droplet SAs than P2 coatings. However, P2 coatings had the best resistance against ink from a permanent marker. The ink that was applied onto optimized P2 coatings immediately shrank into small patches. In addition, these patches of dried ink were readily removed by wiping them with tissue paper, unlike the "permanent" marks that would remain on uncoated glass. In terms of durability, the P2 coatings proved to exhibit greater stability over that of the P1 family of diblock copolymers due to the "liquid-like" state and constant motion of the PFPO block at room temperature.

4.2 Significance of This Work

Amphiphobic and anti-smudge coatings have recently generated significant interest due to their excellent dynamic capabilities of keeping surfaces clean and smudge-free from the natural oils of human skin.[1-3] The optically clear, thin coatings prepared in this thesis may serve as the coatings for self-cleaning windows of skyscrapers or car windshields, or on the screens of iPads® or other small electronic devices. As mentioned earlier, however, preparing such a coating can be quite difficult due to the low surface tension of some oils.[4] It is also challenging to ensure that they are sufficiently durable for certain applications, especially if they are applied onto iPad® screens where the surface is under constant exposure to fingerprints. It should be noted that until now, there have been no reports of diblock copolymer brushes applied onto glass plates that demonstrate these features.

This thesis has described a facile 'grafting-to' approach using block selective solvents to covalently graft and crosslink the diblock copolymers P1-1, P1-2 and P2 onto glass substrates to produce smooth amphiphobic and anti-smudge surfaces. The resultant coatings demonstrated dynamic non-wetting behaviour and the P2 coatings were durable. The FL blocks (PFOEMA and PFPO) in each family

of diblock copolymers provided the low surface energy required for dual liquid repellency, while the GX PIPSMA block became covalently attached onto the glass substrate to form an anchoring layer.

4.3 Future Work

This thesis described the preparation of smooth and optically clear diblock copolymer brush coatings on glass plates that demonstrated amphiphobic and anti-smudge properties. Smooth and chemically homogenous surfaces in combination with a low surface energy surface are key factors in fabricating these films.[5-6] As was previously discussed above, the PFPO block of the P2 diblock copolymer possesses a T_g of -71 ˚C,[7] which provided it with "liquid-like" properties at room temperature and allowed the test droplet to easily slide along the surface.[2]

Although diiodomethane and hexadecane displayed good dynamic properties on these films with low CAH and SA values, a higher SA was required to move the water droplets as they were thought to be attracted to the underlying PIPSMA layer. In the future, it would be worthwhile to increase the molecular weight of the PFPO block to ensure that the anchoring PIPSMA block would be completely covered. In principle, this should provide more CF_3 groups at the surface, and ensure that the lowest possible surface energy is achieved (Figure 4-1a). Increasing the molecular weight of the FL block may also improve the overall dynamic properties of the surface by decreasing the CAH and SA values.

It has been previously reported that an increase in temperature can promote crosslinking and facilitate covalent bond formation between the terminal Si-OH groups of polymers and the hydroxyl groups of various substrates including glass, cotton, and wood.[8-10] During a study conducted by Homuzi *et al.*,[2] they subjected their PFPE-terminated silane compound known as Optool DSX, to a gradual increase in temperature from 25 to 70 ˚C. They immediately observed that the increase in temperature led to a decrease in the CAH, and enhanced the mobility of the test droplets. As is the case with the P2 diblock copolymer examined in this work, Optool DSX possesses a T_g of -116 ˚C that enabled it to exhibit

"liquid-like" behaviour at room temperature, and decreased its viscosity as well as increased the mobility of the PFPE chains as the temperature increased. In a similar study, the mobility of PDMS (T_g = -127 ˚C) chains was investigated as they were subjected to an increase in temperature from 25 to 70 ˚C.[11-12] The enhanced "liquid-like" quality of the film allowed the shearing motion of the sliding test droplet to move the three-phase contact line more readily. If the coatings presented here were heated after the solvent evaporation process, it might improve their dynamic properties since the PFPO chains are similar to those mentioned above (Figure 4-1b). In addition, increasing the temperature may increase the degree of grafting and crosslinking of the PIPSMA block onto the substrate and thus improve the overall durability. Incorporating heat into this system might mimic the act of someone potentially leaving their iPad® or iPhone® inside of their car, or outside in the sun. Therefore, it is important to investigate whether the addition of heat would be beneficial or detrimental to the coatings. If heating did in fact improve the durability and overall dynamic properties, the screens of these devices could be heat-treated before they are assembled.

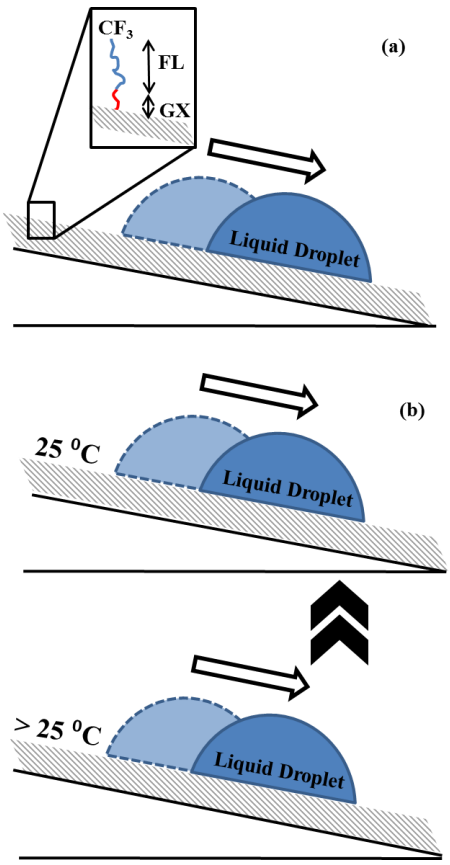

Figure 4-1 A hypothesized graphic representation of a liquid droplet sliding more readily on a glass substrate as the molecular weight of the FL block is increased compared to the GX block (a), and as the temperature in the system is increased above 25 ˚C (b).

In summary, amphiphobic and anti-smudge diblock copolymer brush films were prepared on glass surfaces using block selective solvents. These films were smooth, thin and optically clear, so that they were ideal candidates for coating the screens of small electronic devices such as an iPad® or an iPhone®. Although these coatings were effective, increasing the molecular weight of the FL block, specifically in the P2 diblock copolymer, could dramatically improve the de-wetting capabilities of these coatings. In addition, introducing heat into the system after the solvent had evaporated from the glass plates would allow the test droplets to slide along the surface more readily, as well as improve the durability of the grafted chains.

References

1. Block, S.; Hupfield, P.; Itami, Y.; Kitaura, E.; Kleyer, D.; Masutani, T.; Nakai, Y. New Anti-Fingerprint Coatings. *PCI Magazine* 2008, pp 88-92.
2. Cheng, D. F.; Masheder, B.; Urata, C.; Hozumi, A. *Langmuir* **2013,** *29*, 11322-11329.
3. Urata, C.; Masheder, B.; Cheng, D. F.; Hozumi, A. *Langmuir* **2013,** *29*, 12472-12482.
4. Butt, H.-J.; Semprebon, C.; Papadopoulos, P.; Vollmer, D.; Brinkmann, M.; Ciccotti, M. *Soft Matter* **2013,** *9*, 418-428.
5. Furmidge, C. G. *J. Colloid Sci.* **1962,** *17*, 309-324.
6. Fadeev, A. Y.; McCarthy, T. J. *Langmuir* **1999,** *15*, 3759-3766.
7. Yarbrough, J. C.; Rolland, J. P.; DeSimone, J. M.; Callow, M. E.; Finlay, J. A.; Callow, J. A. *Macromolecules* **2006,** *39*, 2521-2528.
8. Xiong, D.; Liu, G.; Duncan, E. J. S. *Langmuir* **2012,** *28*, 6911-6918.
9. Salon, M.-C. B.; Gerbaud, G.; Abdelmouleh, M.; Bruzzese, C.; Boufi, S.; Belgacem, M. N. *Magn. Reson. Chem.* **2007,** *45*, 473-483.
10. Tshabalala, M. A.; Kingshott, P.; VanLandingham, M. R.; Plackett, D. *J. Appl. Polym. Sci.* **2003,** *88*, 2828-2841.
11. Cheng, D. F.; Urata, C.; Yagihashi, M.; Hozumi, A. *Angew. Chem. Int. Ed.* **2012,** *51*, 2956-2959.
12. Cheng, D. F.; Urata, C.; Masheder, B.; Hozumi, A. *J. Am. Chem. Soc.* **2012,** *134*, 10191-10199.

Appendix A

P1-1/P1-2 and P2 Characterization, Theoretical Calculations, and Supplementary XPS and AFM Data

Diblock Copolymer Characterization. Size exclusion chromatography (SEC) and ^{1}H NMR techniques were used to characterize the previously synthesized diblock copolymers. These synthesis and characterization procedures were conducted by Dr. Muhammad Rabnawaz of the Liu Group. The solvents used for these analyses were TFT (at a flow rate of 1 mL/min), $CDCl_3$:C_6F_6 (3:2, v/v), and $CDCl_3$:TFT (1:3, v/v). From the SEC traces, both the polydispersity indices (M_w/M_n) and the number-average molecular weight (M_n) were measured based on PS standards. ^{1}H NMR was used to measure the block length ratios *n*/*m*, as well as the absolute repeat unit numbers *n* for the PIPSMA blocks of P1-1 and P1-2 by taking the ratio of the intensities of the PIPSMA peak at 0.6 ppm and the initiator peak at 4.1 ppm. These analyses indicated that the samples all had M_w/M_n values that were less than 1.14. In addition, the repeat unit numbers for the first and second blocks were 18 (PIPSMA) and 22 (PFOEMA) for P1-1, 13 (PIPSMA) and 30 (PFOEMA) for P1-2, and 14 (PFPO) and 7 (PIPSMA) for P2, respectively.

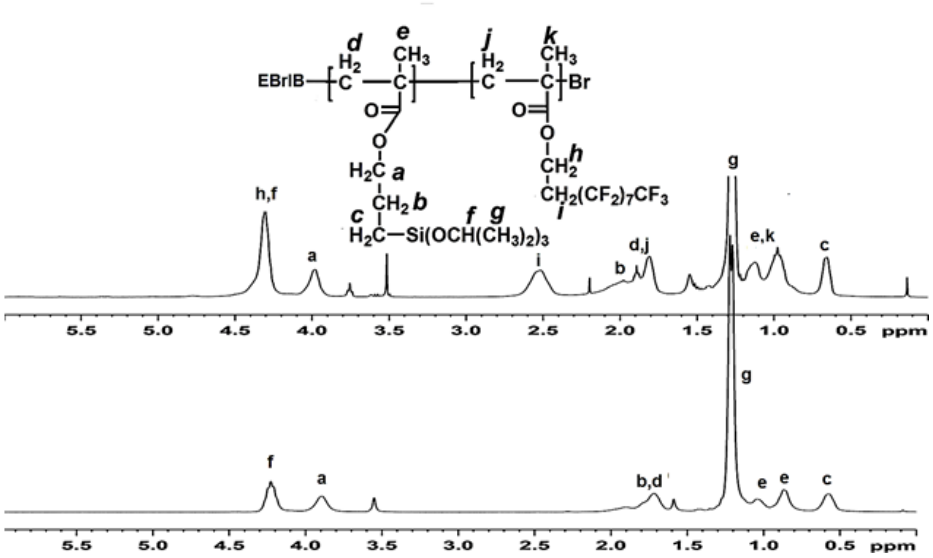

Figure A-1 ^{1}H NMR spectra of P1-1 (top, recorded in $CDCl_3$:C_6F_6 at (3:2, v/v) and its precursor (bottom, recorded in $CDCl_3$) using a 400 MHz spectrometer. The ^{1}H NMR spectrum of P1-2 would appear similar to this spectrum, but the integration ratio would be different.

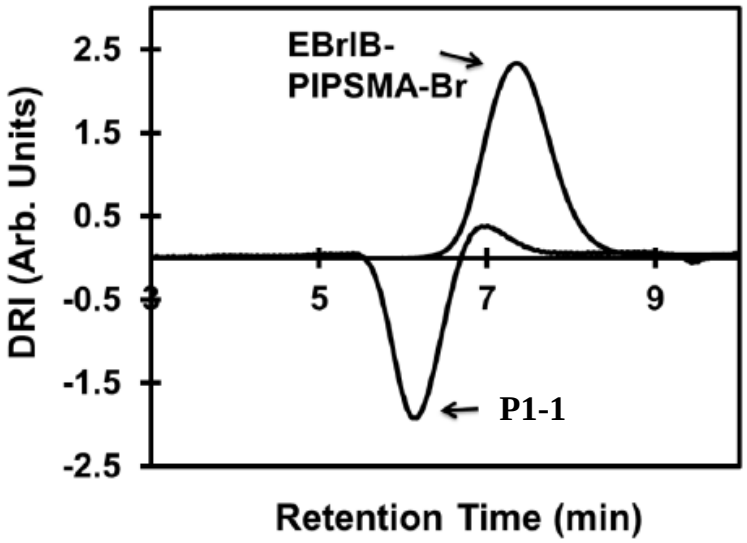

Figure A-2 SEC traces of P1-1 and its precursor. TFT was used as the eluent at a flow rate of 1 mL/min.

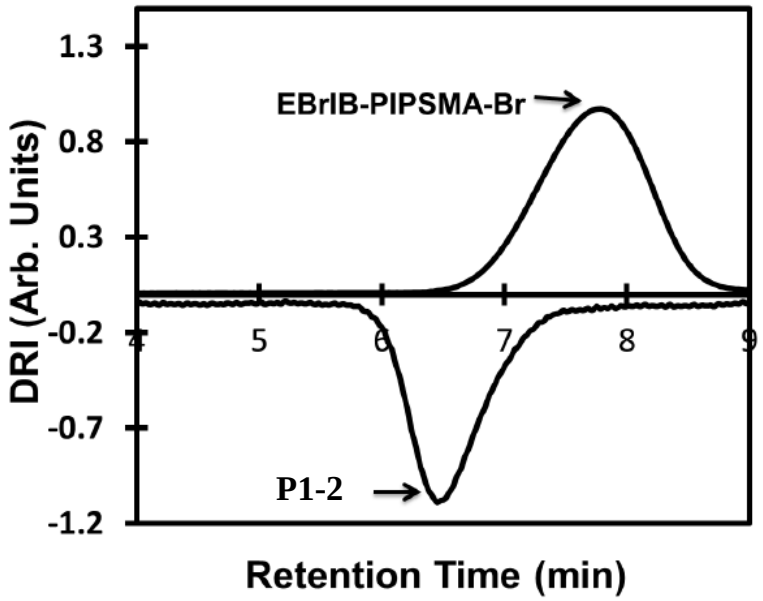

Figure A-3 SEC traces of P1-2 and its precursor. TFT was used as the eluent at a flow rate of 1 mL/min.

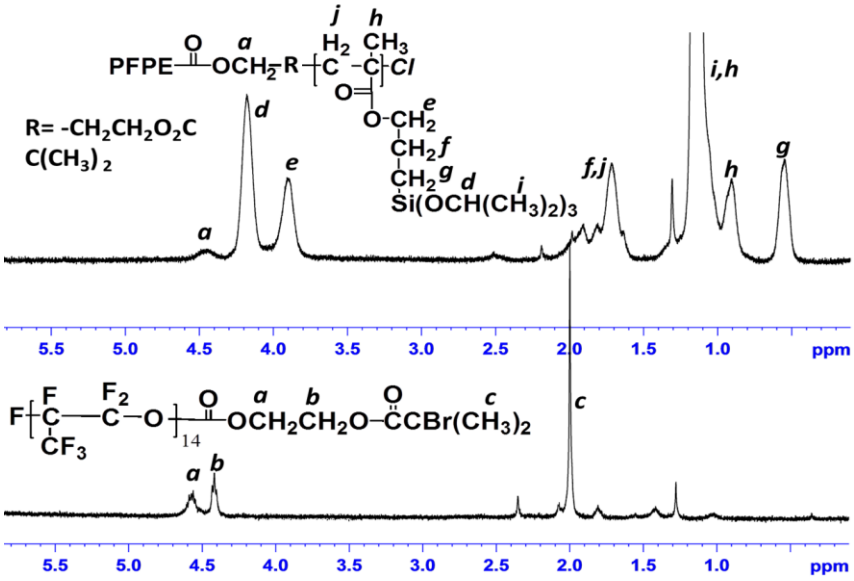

Figure A-4 ^{1}H NMR spectra of P2 (top) and the PFPO precursor (bottom).The samples were recorded in $CDCl_3$:TFT (1:3, v/v) using a 300 MHz spectrometer.

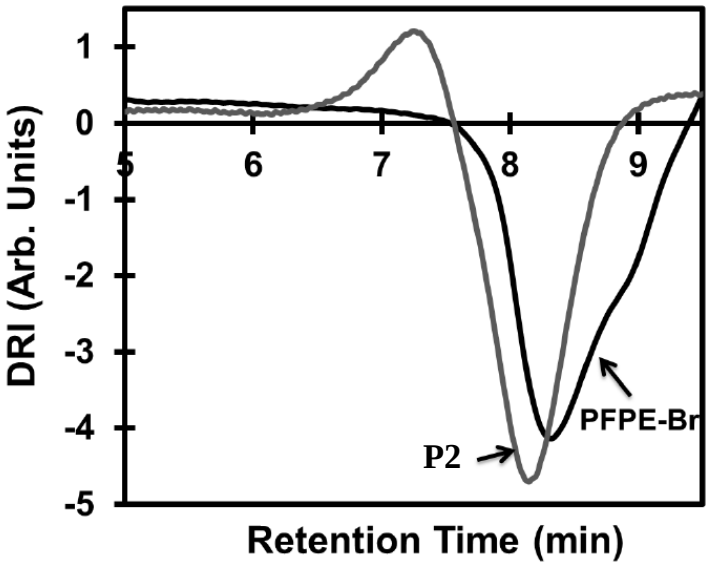

Figure A-5 SEC traces of P2 and its precursor. TFT was used as the eluent at a flow rate of 1 mL/min.

Theoretical Maximum Thickness for P1-2. A P1-2 chain can be viewed as a diblock copolymer chain consisting of PIPSMA and terminal PFOEMA blocks in its backbone.[1] P1-2 incorporates a total of 43 repeat units, and each repeat unit consists of two carbon atoms within the backbone, and thus, n = 86. We assume that the carbon atoms exhibit a zigzag conformation to form the backbone of the copolymer. In addition, a C-C bond length is 0.15 nm and the angle between these bonds is 109.5˚.[2] The contour length of the copolymer backbone can thus be calculated according to Equations (A1) and (A2) where x denotes the length of one segment and l denotes the contour length.

$$\mathrm{Sin}(54.75) = \frac{x}{0.15\ nm} \qquad (A1)$$

$$x = 0.12\ nm$$

$$l = x \times n \qquad (A2)$$

$$l = 0.12\ nm\ \times\ 86$$

$$l = 10.3\ nm$$

The terminal FOEMA unit should be at a tilt angle of 30˚ with respect to the polymer backbone.[3] In reference to the carbon atoms in the FOEMA side chains, we assume a zigzag configuration for the unit. The number of atoms in the unit, n_{PFOEMA}, is 14. Therefore, the length of the PFOEMA unit, (l) can be calculated according to Equation A3:

$$l = \cos(30) \times x \times n_{FOEMA} \qquad (A3)$$

$$l = \cos(30) \times 0.12\ nm\ \times 14$$

$$l = 1.5\ nm$$

Thus, the theoretical maximum chain length of P1-2 will be 11.8 nm. Similar calculations can be employed for P1-1, which yields a theoretical maximum chain length of 11.1 nm.

Theoretical Amount of P1-2 Required to Coat a Surface. P1-2 was used to coat a glass plate with dimensions of 1.0 cm × 1.3 cm. For P1-2 at a maximum thickness (h) of 11.8 nm, the theoretical amount of copolymer needed (m), to coat a glass plate can be calculated. This is accomplished by first calculating the volume (V) of the copolymer according to Equation A4 where V was found to be 15×10^{-7} cm^3.

$$V = w_{glass} \times l_{glass} \times h \qquad (A4)$$

$$V = 1.0\ cm\ \times 1.3\ cm\ \times 11.8\ nm$$

$$V = 15\ \times 10^{-7} cm^3$$

Subsequently, the density (ρ) of the copolymer could be calculated according to Equation A5:

$$\frac{1}{\rho} = \frac{f_{PFOEMA}}{\rho_{PFOEMA}} + \frac{(1 - f_{PFOEMA})}{\rho_{PIPSMA}} \quad (A5)$$

$$\frac{1}{\rho} = \frac{0.877}{1.85\ g/cm^3} + \frac{(1 - 0.877)}{1.82\ g/cm^3}$$

$$\rho = 1.85\ g/cm^3$$

Where the density of the PFOEMA unit was calculated using a method developed within our group to be 1.85 g/cm^3.[4] Meanwhile, the density of the sol-gelled and grafted PIPSMA layer was assumed to be 1.82 g/cm^3.[1] The mass fraction of the PFOEMA unit (f_{PFOEMA}), was calculated to be 87.7 % with a fully-gelled IPSMA block that had an effective formula of $C_7H_{11}O_{3.5}Si$. With these values in hand, ρ was found to be 1.85 g/cm^3.

The amount of copolymer amount, (m) required to coat the glass could then be calculated according to Equation A6:

$$m = \rho \times V \quad (A6)$$

$$m = 1.85\frac{g}{cm^3} \times 15 \times 10^{-7} cm^3$$

$$m = 2.81 \times 10^{-6}\ g$$

Thus, 2.81 µg of P1-2 would be required to cover a glass plate at a film thickness of 11.8 nm. Therefore, for a 1.3 cm^2 sized plate, the copolymer amount was calculated to be 2.2 µg/cm^2. Similar calculations were employed for the P1-1 case. These calculations indicated that 2.67 µg (or 2.0 µg/cm^2) of P1-1 would be needed to cover a glass plate at a film thickness of 11.1 nm.

Theoretical Maximum Thickness of P2. A P2 chain can be viewed as a diblock copolymer chain with a backbone consisting of a PFPO block and a PIPSMA block. The PFPO block incorporates a

total of 14 repeat units, with each repeat unit consisting of two carbon atoms and one oxygen atom. We assumed that the carbon and oxygen atoms exhibited a zigzag conformation to form the backbone of the copolymer. In addition, the C-C bond length would be 0.15 nm, while the C-O bond length would be 0.14 nm. The angle between the bonds is 109.5°.[2] The contour length of the PFPO block can be calculated according to Equation A7, where the length of one C-C segment is expressed as x.

$$\mathrm{Sin}(54.75) = \frac{x}{0.15\ nm} \qquad (A7)$$

$$x = 0.12\ nm$$

Meanwhile, the length of one C-O segment (y) can be calculated according to Equation A8:

$$\mathrm{Sin}(54.75) = \frac{y}{0.14\ nm} \qquad (A8)$$

$$y = 0.11\ nm$$

The contour length (l) can be calculated according to Equation A9:

$$l = (x\ \times 2 + y) \times n \qquad (A9)$$

$$l = (0.12\ nm\ \times\ 2 + 0.11\ nm) \times 14$$

$$l = 4.9\ nm$$

The PIPSMA block incorporates a total of 7 repeat units. Each repeat unit in the backbone consists of two carbon atoms, and thus n = 14. The contour length (l) can be calculated according to Equation A10:

$$l = x \times n \qquad (A10)$$

$$l = 0.12\ nm\ \times 14$$

$$l = 1.7\ nm$$

The total length of the chain can be calculated by adding together the two contour lengths of each block. Thus, the theoretical maximum chain length of P2 will be 6.6 nm.

Theoretical Amount of P2 Required to Coat a Surface. P2 was used to coat a glass plate with dimensions of 1.0 cm × 1.3 cm. For P2 at a maximum thickness (h) of 6.6 nm, the theoretical amount of copolymer required to coat the glass plate can be determined by first calculating the volume of the copolymer (V) according to Equation A11:

$$V = w_{glass} \times l_{glass} \times h \qquad (A11)$$

$$V = 1.0\ cm\ \times 1.3\ cm\ \times 6.6\ nm$$

$$V = 8.6\ \times 10^{-7} cm^3$$

In addition, the density of the copolymer (ρ) can be calculated according to Equation A12:

$$\frac{1}{\rho} = \frac{f_{PFPO}}{\rho_{PFPO}} + \frac{(1 - f_{PFPO})}{\rho_{PIPSMA}} \qquad (A12)$$

$$\frac{1}{\rho} = \frac{0.663}{1.80\ g/cm^3} + \frac{(1 - 0.663)}{1.82\ g/cm^3}$$

$$\rho = 1.81\ g/cm^3$$

Where the density of the grafted PIPSMA layer was assumed to be 1.82 g/cm^3.[1] Meanwhile, the density of the PFPO unit was assumed to be 1.80 g/cm^3. The mass fraction of the PFPO unit (f_{PFPO}) was calculated to be 66.3%, with a fully-gelled IPSMA block that had an effective formula of $C_7H_{11}O_{3.5}Si$. With these values in hand, ρ was found to be 1.81 g/cm^3. The amount of P2 (m) required to coat a glass plates was subsequently calculated according to Equation A13:

$$m = \rho \times V \tag{A13}$$

$$m = 1.81 \frac{g}{cm^3} \times 8.6 \times 10^{-7} cm^3$$

$$m = 1.55 \times 10^{-6}\ g$$

Thus, 1.55 µg (or 1.2 µg/cm^2) of P2 would be required to cover a glass plate at a film thickness of 6.6 nm.

Supplementary XPS and AFM Data.

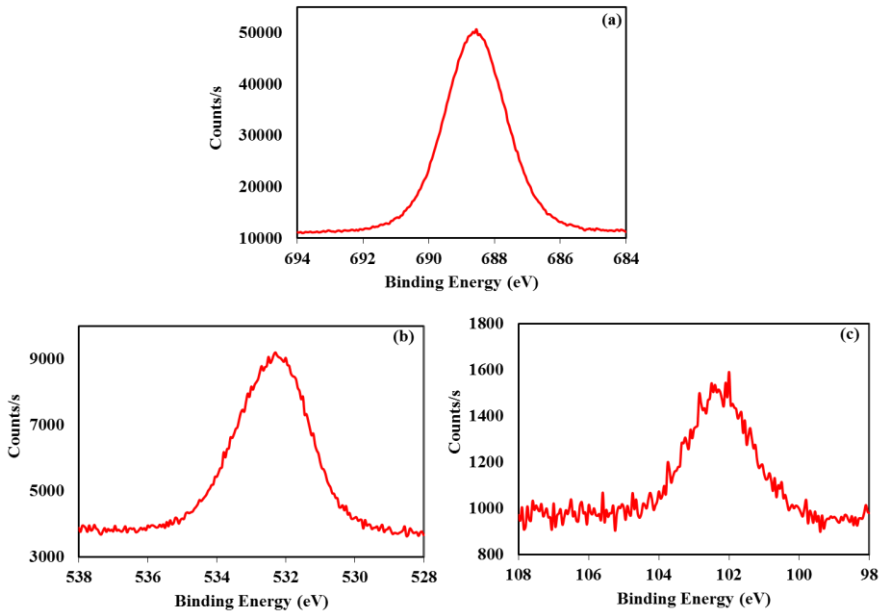

Figure A-6 XPS high resolution F_{1s} (a), O_{1s} (b), and Si_{2p} (c) spectra of the P1-2 coatings that were recorded at an HCl concentration of 0.90×10^{-1} M.[5-6]

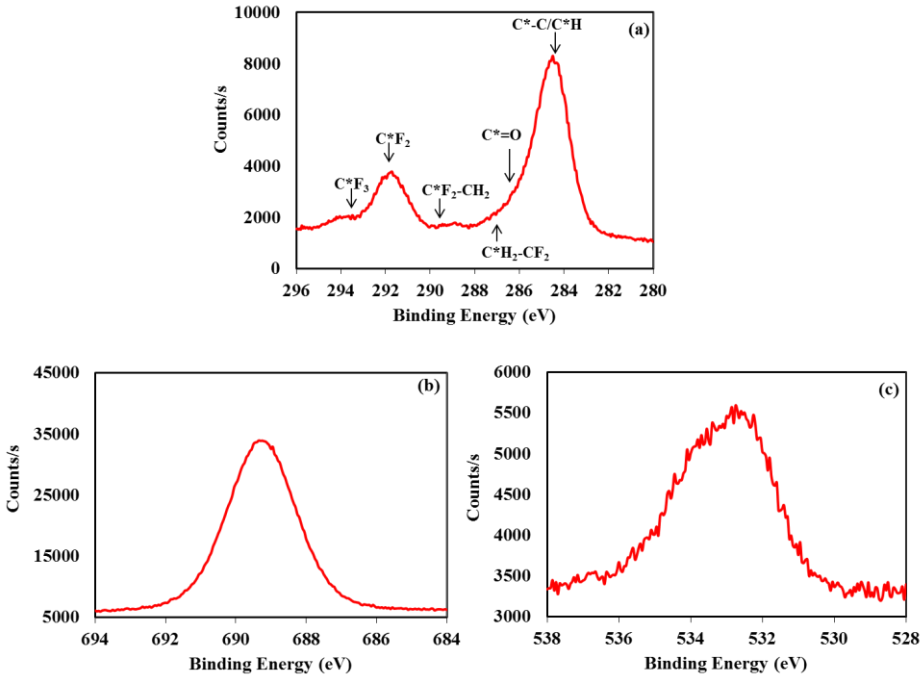

Figure A-7 XPS high resolution C_{1s} (a), F_{1s} (b), and O_{1s} (c) spectra of the PFOEMA homopolymer.[5-6]

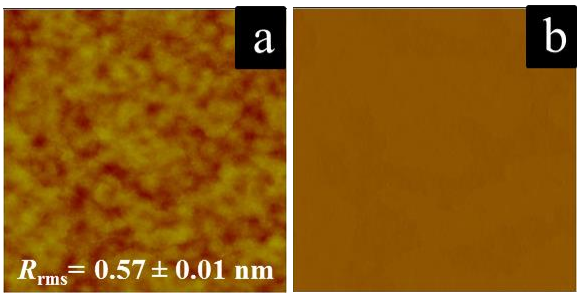

Figure A-8 AFM height (a) and phase (b) images of the PFOEMA homopolymer coated on a glass plate. The height and phase angle delay ranges are 20 nm and 75°, respectively, and the dimensions of the images were 2.0 × 2.0 μm^2.

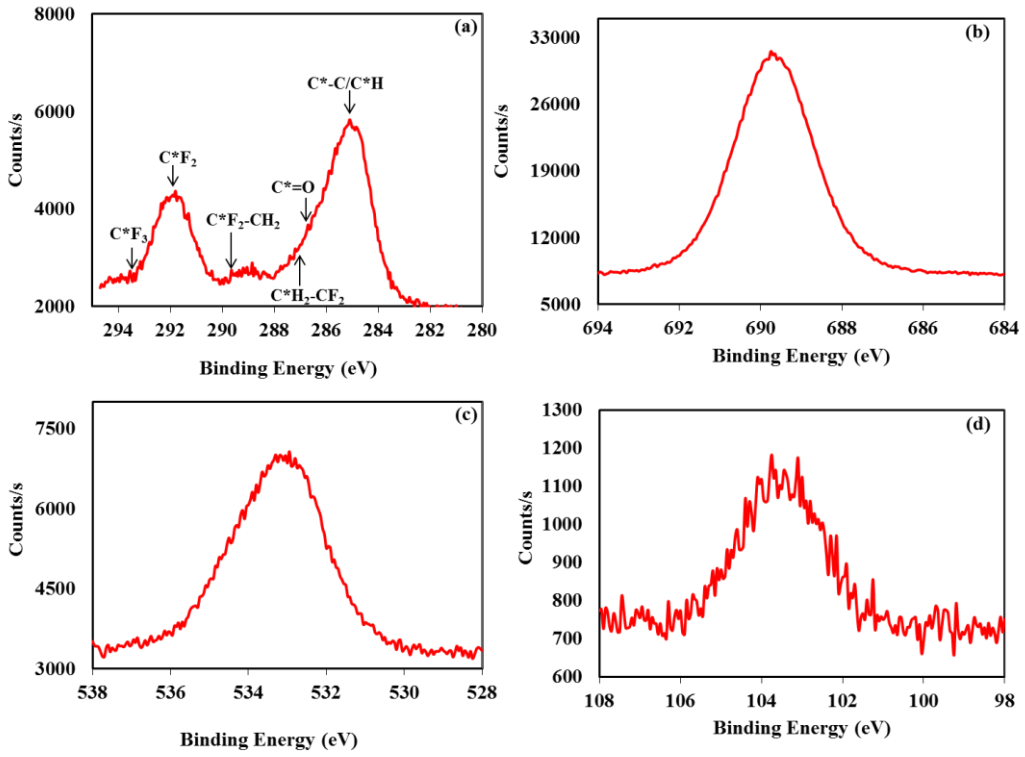

Figure A-9 XPS high resolution C_{1s} (a), F_{1s} (b), O_{1s} (c), and Si_{2p} (d) spectra of the P1-1 coatings that were recorded at an HCl concentration of 0.90×10^{-1} M.[5-6]

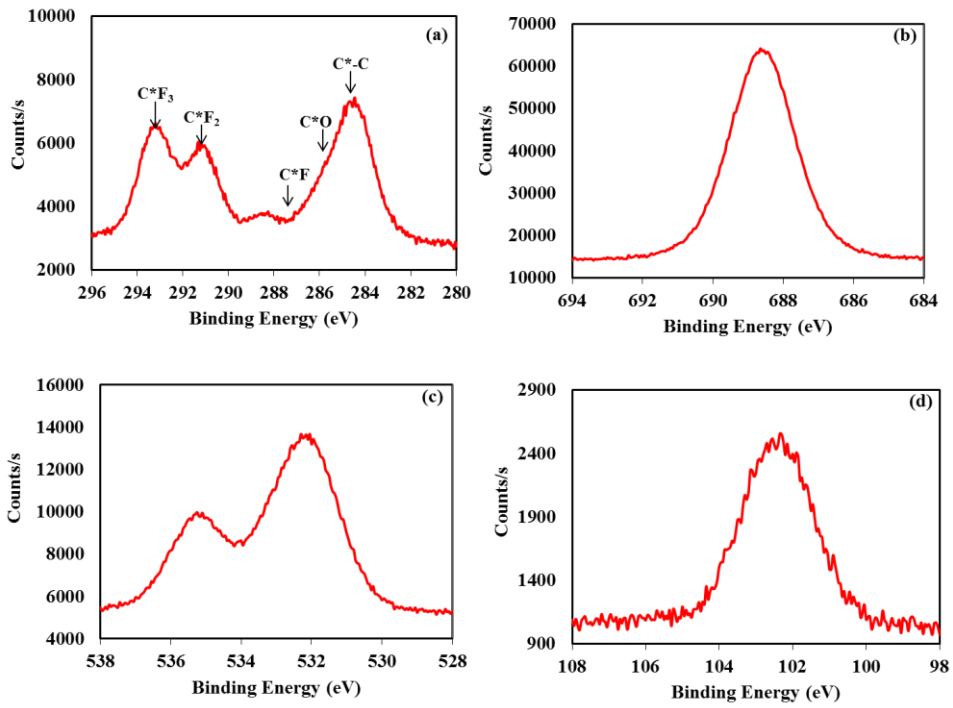

Figure A-10 XPS high resolution C_{1s} (a), F_{1s} (b), O_{1s} (c), and Si_{2p} (d) spectra of the P2 coatings that were recorded at an HCl concentration of 0.90×10^{-1} M.[5-6]

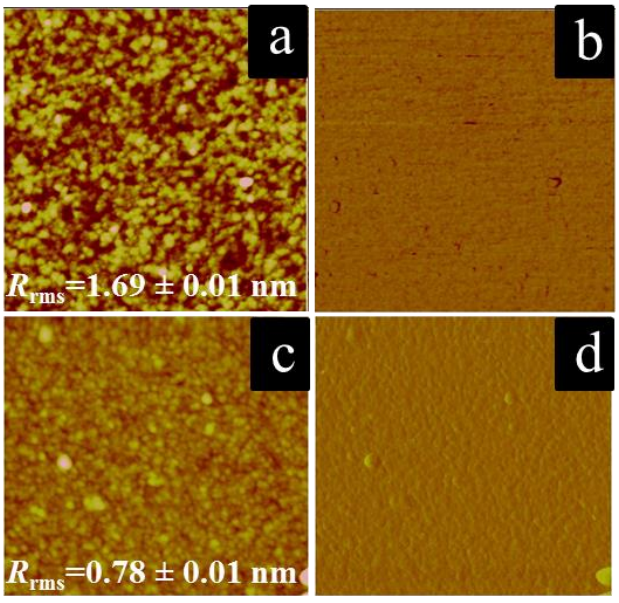

Figure A-11 AFM height (a and c) and phase (b and d) images of the P1-2 coated glass plates before (a and b) and after (c and d) TFT extraction. These plates were coated with an excess copolymer amount of 2.31 µg/cm^2. The height and phase angle delay ranges are 20 nm and 75°, respectively, and the dimensions of the images were 2.0×2.0 µm^2.

References

1. Xiong, D.; Liu, G.; Duncan, E. J. S. *ACS Appl. Mater. Interfaces* **2012,** *4*, 2445-2454.
2. Zhang, D.; Ortiz, C. *Macromolecules* **2004,** *37*, 4271-4282.
3. Hirao, A.; Sugiyama, K.; Yokoyama, H. *Prog. Polym. Sci.* **2007,** *32*, 1393-1438.
4. Kim, J.; Efimenko, K.; Genzer, J.; Carbonell, R. G. *Macromolecules* **2007,** *40*, 588-597.
5. Crist, B. V. *Handbook of Monochromatic XPS Spectra, The Elements of Native Oxides*. XPS International: CA, United States, **1999**.
6. Moulder, J. F.; Stickle, W. F.; Sobol, P. E.; Bomben, K. D. *Handbook of X-Ray Photoelectron Spectroscopy: A Reference Book of Standard Spectra for Identification and Interpretation of XPS Data*. Perkin-Elmer: Boca Raton, FL: **1992**.